Titre: Title:	Solubility Probing of Aqueous FeSO4–H2SO4 and FeSO4–NiSO4 for Hydrometallurgical Applications
Auteur: Author:	Eduarda Depiné Dornelles Da Silva
Date:	2025
Type:	Mémoire ou thèse / Dissertation or Thesis
Référence: Citation:	Depiné Dornelles Da Silva, E. (2025). Solubility Probing of Aqueous FeSO4–H2SO4 and FeSO4–NiSO4 for Hydrometallurgical Applications [Master's thesis, Polytechnique Montréal]. PolyPublie. https://publications.polymtl.ca/71953/

POLYTECHNIQUE MONTRÉAL
affiliée à l'Université de Montréal

Solubility probing of aqueous $FeSO_4-H_2SO_4$ and $FeSO_4-NiSO_4$ for hydrometallurgical applications

EDUARDA DEPINÉ DORNELLES DA SILVA
Département de génie chimique

Mémoire présenté en vue de l'obtention du diplôme de *Maîtrise ès sciences appliquées*
Génie des matériaux

Décembre 2025

POLYTECHNIQUE MONTRÉAL
affiliée à l'Université de Montréal

Ce mémoire intitulé :

Solubility probing of aqueous $FeSO_4-H_2SO_4$ and $FeSO_4-NiSO_4$ for hydrometallurgical applications

présenté par **Eduarda DEPINÉ DORNELLES DA SILVA**
en vue de l'obtention du diplôme de *Maîtrise ès sciences appliquées*
a été dûment accepté par le jury d'examen constitué de :

Daria Camilla BOFFITO, présidente
Jean-Philippe HARVEY, membre et directeur de recherche
Julian SELF, membre et codirecteur de recherche
Kerstin FORSBERG, membre externe

ACKNOWLEDGEMENTS

I would like to acknowledge Professors Jean-Philippe Harvey and Julian Self for their guidance, trust, and encouragement throughout my master's program. I would like to extend my appreciation to Professors Daria Camilla Boffito and Kerstin Forsberg for accepting to be part of the review committee for this project.

To other members of the research group CRCT (Center for Research in Computational Thermochemistry) for their technical and scientific support throughout my master's degree in particular Dyhia Ait Amer, Aidin Barabi, and Kentaro Oishi.

To Jérôme Leroy and Zohra Laimeche from the Laboratory Geo-ingenierie - Geochimie Annalytique at Polytechnique Montreal for the help with AAS analysis.

My family, who constantly demonstrated their presence through constant encouragement and words of affection that reduced the distance between us. To Felipe Michels, who became my family, providing unconditional support at all times.

To all the friends I made during this journey and those I always carry with me. You were essential in ensuring there were many moments of fun, and support.

RÉSUMÉ

Les procédés hydrométallurgiques appliqués au recyclage des batteries lithium-ion reçoivent une attention croissante. Dans ces procédés, des solutions aqueuses complexes de sulfates de métaux de transition apparaissent. Afin d'optimiser la récupération de ces sulfates métalliques par précipitation chimique, des études sont réalisées pour déterminer les limites de solubilité des sulfates de métaux de transition dans l'eau. Le système aqueux contenant du sulfate de fer ($FeSO_4$) et de l'acide sulfurique (H_2SO_4) a été le sujet de plusieurs études qui rapportent une description des limites de solubilité à différentes températures, ainsi qu'une description des phases solides formées. Cependant, les systèmes complexes impliquant la formation de solutions solides et de zones d'immiscibilité, comme le système aqueux contenant du $FeSO_4$ et du sulfate de nickel ($NiSO_4$), n'ont pas été étudiés de manière approfondie en ce qui concerne leurs limites de solubilité. L'objectif de ce travail est de collecter des données expérimentales sur les équilibres solide-liquide de ces deux systèmes ternaires, $FeSO_4$+H_2SO_4 aqueux et $FeSO_4$+$NiSO_4$ aqueux. Le protocole expérimental utilisé consiste à préparer des solutions à des concentrations connues et à les soumettre à des températures inférieures à la température de liquidus, déterminées soit à partir de la littérature, soit calculées à partir des constantes d'équilibre dérivées de la littérature. Après l'établissement de l'équilibre solide-liquide, la composition du liquide saturé a été analysée chimiquement par spectroscopie d'absorption atomique (AAS) et par bilan de masse pour le système aqueux contenant du $FeSO_4$ et du H_2SO_4. Des mesures de solubilité par bilan de masse ont été effectuées pour le système aqueux contenant du $FeSO_4$ et du $NiSO_4$. Ici, l'AAS a été utilisée pour caractériser chimiquement la solution solide formée. Cela a permis de tracer les conodes dans le diagramme de phase isotherme de ce système, ainsi que de caractériser la région solide biphasique, qui est souvent dénommée l'intervalle de miscibilité. La structure cristalline a été analysée par diffraction par rayons X. Il a ainsi été constaté que, d'une manière générale, les structures cristallines formées dans les deux systèmes correspondaient à celles attendues d'après la littérature ou les conodes calculées. Les détails morphologiques préliminaires des cristaux ont également été présentés et comparés aux descriptions disponibles dans la littérature pour les phases mélantérite, szomolnokite et morenosite à l'aide d'un microscope optique. La comparaison des données expérimentales obtenues avec les valeurs de solubilité disponibles dans la littérature pour le système aqueux contenant du $FeSO_4$ et du H_2SO_4 a été satisfaisante. De plus, de nouvelles données d'équilibre solide-liquide pour les systèmes $FeSO_4$, $NiSO_4$ et H_2O (6°C à 10°C) ont été obtenues, en particulier la composition des solutions solides formées pour des concentrations de saturation données a été déterminée.

ABSTRACT

Hydrometallurgical processes applied to the recycling of lithium-ion batteries have been receiving increasing attention. In such processes, complex aqueous solutions of transition metal sulfates appear. To optimize the recovery of these metal sulfates through chemical precipitation, studies have been conducted to investigate the relevant aqueous transition metal sulfate solubility limits. The aqueous system containing iron sulfate ($FeSO_4$) and sulfuric acid (H_2SO_4) is one of the systems that has received attention over the years. It has a description of solubility limits at various temperatures, as well as a description of the solid phases formed. However complex systems involving the formation of solid solutions and regions of immiscibility, such as the aqueous system containing $FeSO_4$ and nickel sulfate ($NiSO_4$) have not been explored as extensively in terms of their solubility limits. The objective of this work is to collect experimental data on the solid-liquid equilibria of these two ternary systems, aqueous $FeSO_4$+H_2SO_4 and aqueous $FeSO_4$+$NiSO_4$. The experimental protocol used includes preparing solutions at known concentrations, and submitting them to temperatures below the liquidus temperature, determined either from literature or computed from the literature-derived equilibrium constants. Following, establishment of solid-liquid equilibrium, the composition of the saturated liquid was chemically analyzed using atomic absorption spectroscopy (AAS) and material balance for the aqueous system containing $FeSO_4$ and H_2SO_4. Material balance solubilty measurements were undertaken for the aqueous system containing $FeSO_4$ and $NiSO_4$. Here, AAS was used to chemically characterize the solid solution formed. This allowed drawing of the tie lines in the isothermal phase diagram of this system, as well as characterizing the biphasic solid region, often described as the miscibility gap. The crystal structure was further analyzed using X-ray diffraction. As a result, it was found that, in general, the crystal structures formed in both systems agreed with those expected from the literature or computed tie lines. Preliminary morphology details of the crystals were also provided and compared against the literature descriptions for the melanterite, szomolnokite, and morenosite phases using an optical microscope. Comparison of the acquired experimental data to literature solubility values for the aqueous system containing $FeSO_4$ and H_2SO_4 was successful. Furthermore, new solid-liquid equilibria data for $FeSO_4$, $NiSO_4$ and H_2O systems (6°C to 10°C) was acquired, specifically the compositions of solid solutions formed for given saturation concentrations were resolved.

TABLE OF CONTENTS

LIST OF TABLES

LIST OF FIGURES

LIST OF ACRONYMS AND NOTATION

DSC Differential Scanning Calorimetry

AAS Atomic Absorption Spectroscopy

LIB Lithium-ion batteries

XRD X-Ray Diffraction

CALPHAD Calculation of Phase Diagrams

MCMB Mesocarbon Microbeads

S_1 Melanterite as solid phase

S_2 Morenosite as solid phase

S_3 Szomolnokite as solid phase

L Liquid phase

F23H1 Sample containing 23.0 wt% of $FeSO_4$ and 1.55 wt% of H_2SO_4

F17H10 Sample containing 17.0 wt% of $FeSO_4$ and 10.69 wt% of H_2SO_4

F13H26 Sample containing 13.0 wt% of $FeSO_4$ and 26.3 wt% of H_2SO_4

F11H27 Sample containing 11.0 wt% of $FeSO_4$ and 27.0 wt% of H_2SO_4

F8H30 Sample containing 8.00 wt% of $FeSO_4$ and 30.9 wt% of H_2SO_4

LIST OF SYMBOLS

w_i^{crystal} Mass of species i in the crystal (g)

$n_{\boldsymbol{i}}^{\text{crystal}}$ Number of moles of species i in the crystal (mol)

$M_{i,e}$ Molar mass of species i or elements e (g/mol)

$w_{\boldsymbol{i}}^{\text{liquidus}}$ Mass of species i in the liquid solution at $T = T_{\text{liquidus}}$ (g)

$w_{\boldsymbol{i}}$ Mass of species i in the liquid solution at $T > T_{\text{liquidus}}$ (g)

T Temperature (°C)

T_{liquidus} Liquidus temperature (°C)

C_e^{Diluted} Concentration of elements e in the diluted solution (g/L)

C_i^{Initial} Concentration of species i in the diluted solution (g/L)

ϕ_i Concentration of species i in the initial solution (wt%)

f^{Initial} Dilution factor

w^{liquidus} Total mass in the liquid solution at $T = T_{\text{liquidus}}$ (g)

w_{Tot} Total mass in the liquid solution at $T > T_{\text{liquidus}}$ (g)

$\mu_{(\text{e,i})}$ Chemical potential of elements e in species i

$\ln K_{\text{SP(e,i)}}$ Solubility product constant of elements e in species i

$n_{\boldsymbol{e}}^{\boldsymbol{i}}$ Number of moles of elements e in species i

CHAPTER 1 INTRODUCTION

The demand for Lithium-ion batteries (LIB) is expected to grow, and as such recycling processes are expected to hold increasing importance [1]. The two main recycling process categories are pyrometallurgical and hydrometallurgical [2, 3]. Hydrometallurgical processes have the possibility to reduce energy consumption versus pyrometallurgy, and potentially allow easier recovery of lithium. However, this will depend on process optimisation regarding for example flowsheet complexity and reagent schemes [1]. Following the battery discharge, recycling routes involve the mechanical and thermal treatment, where plastic materials, carbon anodes, and some metals are separated [4]. For the hydrometallurgical processes specifically, the materials used in the battery cathode undergo leaching, which most commonly use sulfuric acid H_2SO_4 as a leaching agent, followed by separation and purification [1, 4]. Depending on the type of cathode used in the battery, the respective chemical composition of the resulting sulfate leachate will be altered and thus can change the chemical precipitation step. [4].

Possible compositions include Li, Ni, Co, Al, Fe, among others. Generally, the concentration of elements such as Fe and Al in the leachate solution is low, and thus they are removed during the purification phase [1,4]. In the case of Fe, purification occurs mainly through precipitation using different agents such as oxygen, CaO, or NaOH, for example [1, 4, 5]. The effectiveness of this step depends greatly on the industrial processes used. After purification of impurities (Fe, Al, etc.), Ni and Co could be separated [1]. Common methods include solvent extraction or selective precipitation, generating solutions rich in Ni or Co [4]. Thus, the Ni-rich solution, for example, undergoes crystallization to yield the solid $NiSO_4 \cdot 6\,H_2O$, usually through solvent evaporation or methodologies such as crystallization at low temperatures to avoid problems caused by the high concentration of sulfuric acid [4, 6].

The viability of hydrometallurgical recycling will depend on the optimization of the various flowsheet processes. To optimize the recovery of metals in crystallization processes after acid leaching, the behavior of metals dissolved in the aqueous solution must be known. Solubility diagrams can serve as a guide for this purpose [4]. The description of the solubility in aqueous media of metals present in the acidic leaching solution is well known when considering binary systems; however, when adding a new component to the system, there is often a lack of available solubility data. Among these metals are iron (Fe) which is often in the form of impurity, and nickel (Ni), which have their respective sulfates as by-products of the leaching process [4].

The solubility diagrams of iron sulfate ($FeSO_4$) and nickel sulfate ($NiSO_4$) in water are well described in the literature [7–13]. When sulfuric acid is added to these binary systems, different authors have studied the solubility limits [9, 10, 14–18]. In fact, for the ternary system containing $FeSO_4 - H_2SO_4 - H_2O$, different temperatures and methodologies have been reported [14–18]. However, when the ternary system is composed of the two transition metal sulfates in water, to our knowledge, only Charykova *et al.* (2010) and Balarew *et al.* (1973) have reported their solubility diagram and mentioned the possibility of solid solution formation, in addition to a possible miscibility gap region [19,20]. It is therefore important to conduct a more extensive study of the solubility diagram and the behavior of iron and nickel sulfates in water, given that limited research has been done on this subject to date. So, defining a solubility measurement method, evaluated by a well-established system, can contribute to generating data for those who have limited literature.

The definition of the preferable methodology to be adopted varies according to the characteristics of the system and properties of interest [21]. In the case of aqueous systems, three different methods may be employed. In analytical methods, the composition, temperature, and pressure of the system are kept constant until equilibrium is reached and the saturated solution and solid are characterized [21–23]. Synthetic methods, on the other hand, vary a property as a new equilibrium is reached until the solid-liquid equilibrium is identified [21–23]. Among the properties that can be associated with solubility diagrams are thermal, electrical, optical, or chemical properties, which can be obtained through different techniques [22, 23].

In this work, the synthetic method with constant composition and temperature variation was defined for the $FeSO_4 - H_2SO_4 - H_2O$ system. The analysis of the saturated solution obtained at temperatures below the liquidus temperature was performed using Atomic Absorption Spectroscopy (AAS) and material balance, while the crystal structure of the crystal formed was analyzed using X-Ray Diffraction (XRD). With the evaluation of the methodology through data analysis and comparison with the literature, the same methodology was followed for the $FeSO_4 - NiSO_4 - H_2O$ system, where the saturated solution was analyzed through material balance and the solid, besides the XRD analysis, was analyzed by AAS. Thus, the main objective is to provide experimental data on the solubility limits of the $FeSO_4 - NiSO_4 - H_2O$ system, given the limited availability observed during the research.

CHAPTER 2 LITERATURE REVIEW

2.1 Solubility measurement techniques

The understanding of the solubility limits of a system is important because it is a thermodynamic property of equilibrium and also enables different practical applications [21]. For example, studies are being conducted to increase the solubility of pharmaceutical active ingredients so that their gastrointestinal absorption is optimized [24, 25]. Or, as is the motivation for this work, the study of the solubility of sulfates in aqueous systems can enable the recycling of LIB's [4]. Different techniques can be used to obtain experimental data on solubility limits, but all of them require good practices. [23]. This section aims to list some of the methods employed, as well as considerations to be adopted to ensure good practices.

Regardless of the method chosen, certain variables in the solubility measurement methodology must be considered in order to best describe the systems under study. These aspects include the presence of impurities, temperature fluctuations, and the correct determination of thermodynamic equilibrium [23]. The measurement sensitivity depends on the technique used. For example, techniques associated with conductivity have been shown to be more sensitive to the presence of impurities [23]. Sun *et al.* (2015) studied the effect of the presence of different chloride salts (Na, Ca, Mg, and Al) on the solubility of the aqueous system containing $CaSO_4 \cdot 2\,H_2O$. In the study, it was possible to observe an increase in solubility even with small amounts (0.05 molality) of the chloride salts, with the exception of Ca, where the common ion mechanism acted to reduce solubility [26]. Temperature fluctuations can also lead to incorrect data acquisition due to the long period of time required to achieve equilibrium [21,23]. Although there is no consensus on the temperature change value above which it is no longer considered a fluctuation but a variation, it is believed that values above 2°C can already be classified as a variation [21–23]. Temperature variations can lead to alterations in the solubility limits studied, as well as in the equilibrium phases. Different authors who studied the $FeSO_4 - H_2SO_4 - H_2O$ system reported solubility in a temperature range from -20°C to 100°C [14, 15, 17, 27, 28]. It can be observed that with increasing temperature, the saturation concentrations of $FeSO_4$ for the melanterite ($FeSO_4 \cdot 7\,H_2O$) formation conditions are higher, which is the opposite effect of that mentioned for szomolnokite ($FeSO_4 \cdot H_2O$). It is also possible to observe the influence of temperature in the transition point between phases, shifted to lower concentrations of H_2SO_4 as the temperature increases [14, 15, 17, 27, 28]. Finally, the correct establishment of thermodynamic equilibrium can be determined through studies of chemical composition measurements over time using agitation. For example, the study by

Ait Amer (2023) investigated the dissolution kinetics of systems containing $FeSO_4 - H_2O$ and $CoSO_4 - H_2O$ at different temperatures [29].

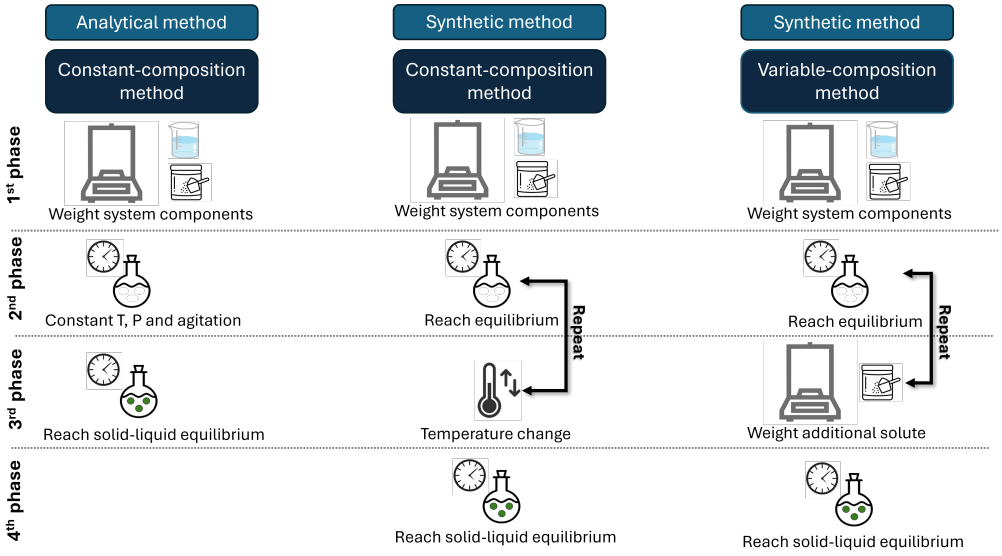

Figure 2.1 Representation of different methods of measuring solubility [21–23].

The methods for measuring solubility can be divided into two categories: analytical or synthetic methods. Analytical methods are defined as those in which a given composition of the system, supersaturated or with excess solute, is subjected to experiments and characterizations under isothermal and isobaric conditions [21, 22]. Synthetic methods are those in which, as the equilibrium of a prepared solution is reached, a property is measured and a new variation in temperature, composition, or pressure is made and then a new equilibrium is reached and the property is measured again [21, 22]. This property can be chemical, electrical, optical, thermal, among others. A new division can be made regarding the chemical composition of the system, which can be constant during the experiment, under variation of another condition of the system, or the composition can be variable while other properties are constant [23]. In summary, analytical methods can also be considered as having a constant composition, but synthetic methods may or may not contain variation in their chemical composition. Figure 2.1 illustrates the different methods that can be employed.

As an example of the analytical method and constant composition presented in Figure 2.1, the protocol established by Bullough *et al.* (1952), described in Table 2.1, can be mentioned [14]. The objective of the Bullough study was to measure the solubility of $FeSO_4$ in different concentrations of H_2SO_4 and H_2O. To this end, the authors mention that it was necessary to maintain agitation at a constant temperature for about 3 to 15 days for equilibrium to be reached, which is the main disadvantage associated with this methodology

[14, 22]. Currently, the same methodology used by Bullough *et al.* (1952) can be called the shake-flask method, which was also used by Baka *et al.* (2007) to analyze the solubility of a pharmaceutical species in a buffer solution and optimize the protocol [30]. Despite the similar methodology for obtaining the solid-liquid equilibrium solution, the analysis of the saturated solution was different between the two authors mentioned, being performed by titration by Bullough *et al.* (1952) and by UV-Vis spectrophotometry by Baka *et al.* (2007) [14, 30]. Other techniques can also be used for chemical characterization without altering the solubility measurement methodology, such as gravimetry, Inductively Coupled Plasma (ICP), and AAS.

The category of synthetic methods with constant composition can be exemplified by the cloud method and the cooling and heating curves method [23]. The cloud method consists of applying temperature variations to a solution of known and constant composition to verify the temperature at which the phase change occurs, for example from one to two phases in equilibrium in the system [23]. Belopol'skii *et al.* (1948) used this technique in their methodology, where the temperature at which the change from liquid to solid-liquid equilibrium occurred was observed visually [17]. Variations of this same methodology can be employed with the use of microscopes, spectrophotometers, or turbidimeters, for example. In addition, the identification of an abrupt change in the slope of heating and cooling curves can be used as a technique for identifying the saturation temperature of a system of known composition [23]. This method can be implemented simply, with the assistance of a thermocouple or through the use of more sophisticated techniques such as Differential Scanning Calorimetry (DSC) or Differential Thermal Analysis (DTA) [23]. Kousksou *et al.* (2007) aimed to describe how DSC can be used to obtain the liquidus temperature in the alcohol-ethanol system [31].

The third possibility presented in Figure 2.1 is the combination of the synthetic methodology with variable composition. Starting from an initial composition solution, a property is kept constant until equilibrium is reached, at a point in which a new amount of solute is added and a new equilibrium is reached [22, 23]. The procedure is repeated until a second phase is identified. The property to be kept constant can be thermal, optical, or electrical [22]. An example of this method is the experiment conducted by Zhou *et al.* (2018), where the systems $FeSO_4 - H_2SO_4 - H_2O$ and $FeSO_4 - H_2SO_4 - HCl - H_2O$ systems were evaluated for solubility at temperatures of 10, 17, and 35°C while the composition of $FeSO_4$ was increased until solid-liquid equilibrium was established [16].

The saturated solution can be analyzed chemically, depending on the solubility measurement technique, through ICP, AAS or laser induced breakdown spectroscopy. After the

separation of the crystal, it can be submitted to chemical analysis, examples include Energy-Dispersive X-ray Spectroscopy (EDS) or by diluting the crystal and subsequently subjecting it to ICP or AAS analysis. The crystal can also be analyzed in terms of its morphology using optical microscopy or more advanced techniques such as Scanning Electron Microscopy (SEM). Furthermore, the structure of the phase formed can be identified using XRD technique [21, 23].

2.2 Binary Systems

Binary systems are described as those in which there is a mixture of two components that could be in differents states, namely: solids, liquids, or gases [32, 33]. The influence of adding a second component on the properties of a first component is described through phase diagrams, which reflect the equilibrium of properties in a mixture [32,33]. Temperature-composition diagrams show the influence of temperature on the composition of phases that are in equilibrium at some imposed pressure, which can be described by one or more states [32, 33]. Among the possibilities of equilibrium, the presence of both phases solid and liquid is commonly referred to as solid-liquid equilibrium [32, 33].

The solid-liquid equilibrium is associated with the solubility of the mixture; in other words, the equilibrium refers to the saturation of a liquid. Saturation is determined when an undissolved solute is in equilibrium with the dissolved solute [32]. This equilibrium can be determined through the chemical potentials of species, which is constant for a species in equilibrium between two phases [34]. Importantly, to properly describe solid-liquid equilibria, it is important to know the chemical nature of the species in possible equilibrium, including the stoichiometry of solids to be considered [35].

Solid-liquid equilibrium can be represented by a solubility graph, usually plotted with the composition variation of one of the components on the vertical axis and the temperature variation on the horizontal axis [32, 33]. In this type of diagram, information about the saturation of a phase in the liquid state and its dependence on the temperature and composition of the mixture is easily obtained, in addition to providing a description of the solid phases formed [32, 33]. Two types of solids are here considered for solid-liquid equilibrium: solids of fixed composition and solid solutions [32, 33]. When solid solutions are formed, this complicates the solid-liquid equilibria given the variable composition of the solid that can be formed [36].

2.2.1 Aqueous solution modelling

One of standard modelling approaches to study solid-liquid equilibria for binary aqueous solutions (electrolyte with one dissolved salt) are the Pitzer equations. These allow a description of the activities of species in the aqueous phase [34, 37]. We note that these equations have also been extended for use to ternary systems (see subsections 2.3.1 and 2.3.2) [10, 19, 27, 38]. In order to calculate phase equilibria based on a thermodynamic model, such a model comprised of the Pitzer equations, the Calculation of Phase Diagrams (CALPHAD) approach is often used [39, 40]. It allows resolution of phase equilibria for binary as well as higher order systems (e.g. ternary and above) through numerical calculations to minimize the Gibbs energy of the studied system.

2.2.2 Iron Sulfate - Water

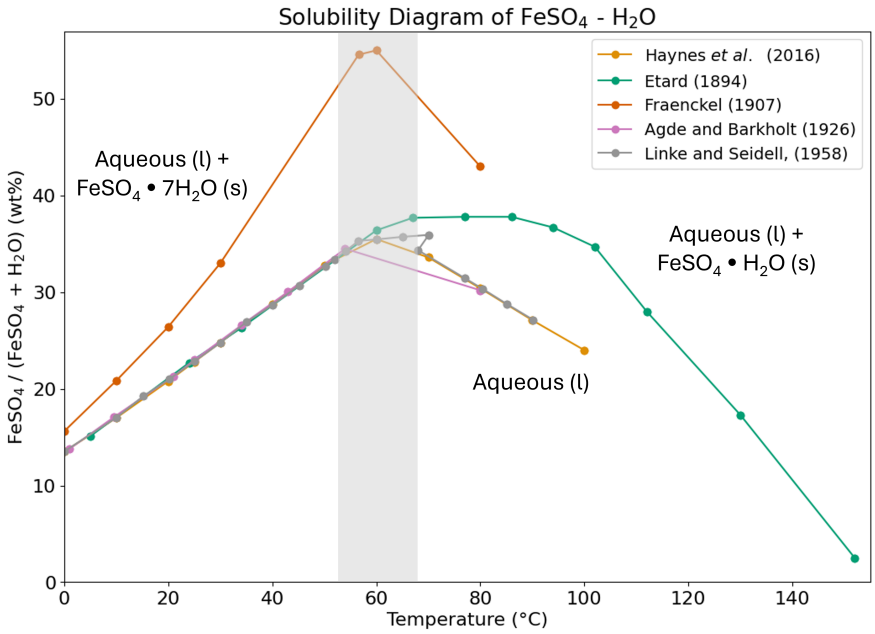

Figure 2.2 Literature data on solubility diagram for $FeSO_4 - H_2O$ system [7, 8, 11–13]. Circles are experimental data and lines are only included for visual ease. Gray area represents the lowest and highest solid phase change temperature values reported by the authors.

The first region described in Figure 2.2 is related to the formation of the heptahydrated solid phase of iron sulfate, denominated melanterite, which can be described by the following equilibrium (Equation 2.1):

$$FeSO_4 \cdot 7\,H_2O\,(s) \rightleftharpoons Fe^{2+}\,(aq) + {SO_4}^{2-}\,(aq) + 7\,H_2O\,(l) \tag{2.1}$$

The presence of the monohydrate phase of iron sulfate denominated szomolnokite is favored from temperatures between 56°C and 65°C, range described in gray in the Figure 2.2, following the equilibrium below (Equation 2.2) :

$$FeSO_4 \cdot H_2O\,(s) \rightleftharpoons Fe^{2+}\,(aq) + {SO_4}^{2-}\,(aq) + H_2O\,(l) \tag{2.2}$$

From the solubility data presented and also from other authors, Kobylin *et al.* (2011) thermodynamically modeled the $FeSO_4 - H_2O$ system [41]. The result of this model was the formation of a phase diagram between temperatures of -25°C and 225°C as a function of the mass fraction of $FeSO_4$ from 0 to 0.5 [41]. In their work, the transition point between the melanterite and szomolnokite phases was calculated at 56.5°C and mass fraction of 0.352 [41]. Furthermore, the eutectic point was calculated at -1.96°C and mass fraction of 0.133, between a mass fraction of 0 to the eutectic point, the aqueous solution is in equilibrium with the ice [41]. Kobylin *et al.* (2011) also reported for temperatures below the eutectic point the thermodynamic equilibrium between melanterite and ice [41].

2.2.3 Nickel Sulfate - Water

As for the previous binary system, various authors have reported solubility limits for the aqueous nickel sulfate system. Authors such as Jambor *et al.* (2000) and Linke and Seidell (1958) summarized experimental results reported in the literature, while Kobylin (2011) modeled this system thermodynamically [8, 10, 42, 43]. Figure 2.3 shows some of the solubilities reported in the literature. The data presented by Haynes *et al.* (2016), Linke and Seidell (1958), Ma *et al.* (2021), and Reardon (1989) show similar $NiSO_4$ concentrations as the solubility limit between temperatures of 0°C and 100°C [7–10]. The transition point between the formation of morenosite ($NiSO_4 \cdot 7\,H_2O$) to retgersite (α-$NiSO_4 \cdot 6\,H_2O$) were reported at 32°C by Linke and Seidell (1958) and at 40°C by Reardon (1989), while the transition point between retgersite and nickelhexahydrite (β-$NiSO_4 \cdot 6\,H_2O$) was reported at 54.5°C and 60°C by the respective authors [8, 10].

In Figure 2.3, the three main solid-liquid phases are reported. The first one shows the formation of morenosite, the heptahydrated structure of nickel sulfate, as demonstrated in Equation 2.3 below:

$$NiSO_4 \cdot 7\,H_2O\,(s) \rightleftharpoons Ni^{2+}\,(aq) + {SO_4}^{2-}\,(aq) + 7\,H_2O\,(l) \tag{2.3}$$

The second equilibrium shown in Figure 2.3 is the formation of the alpha phase of the

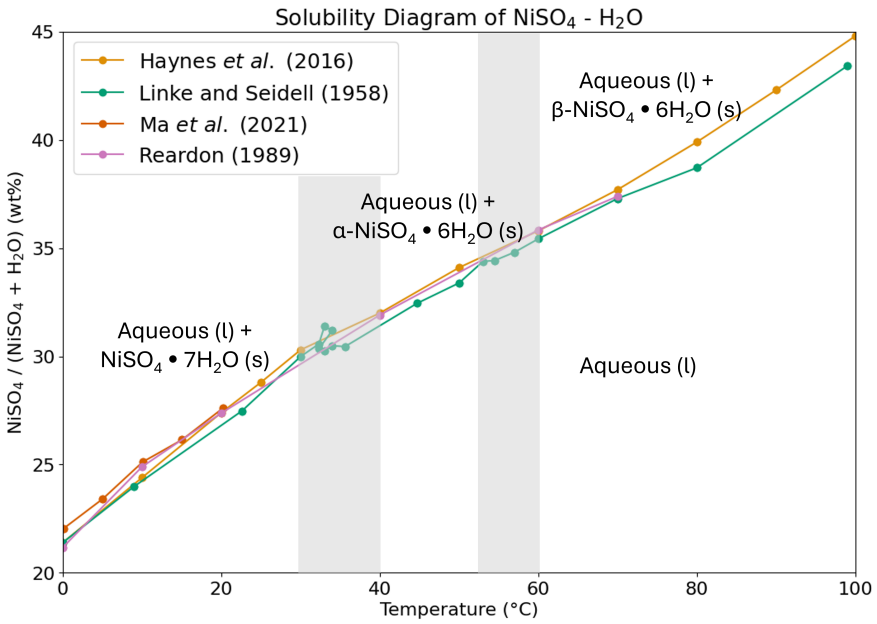

Figure 2.3 Literature data on the solubility diagram for the nickel sulfate - water system [7–10]. Circles are experimental data and lines are only included for visual ease. Gray area represents the lowest and highest solid phase change temperature values reported by the authors.

hexahydrate structure of nickel sulfate, retgersite. Its respective equilibrium equation is as follows (Equation 2.4):

$$\alpha\text{-NiSO}_4 \cdot 6\,\text{H}_2\text{O}\,(\text{s}) \rightleftharpoons \text{Ni}^{2+}\,(\text{aq}) + \text{SO}_4{}^{2-}\,(\text{aq}) + 6\,\text{H}_2\text{O}\,(\text{l}) \tag{2.4}$$

The third structure formed from the solid-liquid equilibrium is nickelhexahydrite, formed by the beta structure of nickel sulfate hexahydrate, represented by the Equation 2.5:

$$\beta\text{-NiSO}_4 \cdot 6\,\text{H}_2\text{O}\,(\text{s}) \rightleftharpoons \text{Ni}^{2+}\,(\text{aq}) + \text{SO}_4{}^{2-}\,(\text{aq}) + 6\,\text{H}_2\text{O}\,(\text{l}) \tag{2.5}$$

For the purpose of developing a thermodynamic model, Kobylin (2011) used the data presented here along with data from several other authors with the aim of expanding the $NiSO_4 – H_2O$ system models to temperatures up to 220°C [43]. As a result of his work, a phase diagram for temperatures between -25°C and 220°C was plotted [43]. The point at 28.4°C and 2.83 mol/kg H_2O was calculated as being the transition point between the aqueous phase, morenosite, and retgersite [43]. The transition point between the aqueous phase, retgersite, and nickelhexahydrite was identified at 54°C and 3.55 mol/kgH_2O [43]. From 91.5°C onward,

the monohydrated structure of nickel sulfate dwornickite is formed [43]. Furthermore, the eutectic point of ice, aqueous solution, and morenosite was defined at -3.18°C and 1.62 mol/kg H_2O [43].

2.3 Ternary Systems

Ternary systems are comprised of three components. The addition of a third component affects the thermodynamic properties of the system, as mentioned for the addition of a second component in section 2.2. The graphical representation of phase diagrams in ternary systems is modified when compared with that mentioned for binary systems. The phase diagrams for ternary systems can be reported based on constant temperature and pressure in a triangular format, where each axis represents a component composition or, when there is a variation in temperature or pressure, the diagram becomes a triangular prism. Consequently, the graphical representation of solubility diagrams can vary, since two properties must be kept constant, i.e., temperature or composition of any of the three components in the system. In ternary systems, the types of solid phases that can be formed may be solids of fixed composition or solid solutions, as as described in the section 2.2.

2.3.1 Iron Sulfate - Sulfuric Acid - Water

One of the ternary systems studied in this work is the solution of iron sulfate ($FeSO_4$), sulfuric acid (H_2SO_4) and water (H_2O). The formation of iron sulfate is usually subsequent to the leaching process with sulfuric acid, where Fe is usually impurity [4]. Different authors have studied the solubility limit of iron sulfate in different dilutions of sulfuric acid in water [14–18]. Therefore, different solubility curves have been reported and Figure 2.4 summarizes some of the results obtained between the temperatures of 17°C to 30°C. Within these temperature ranges and compositions up to 70 wt% of H_2SO_4, the formation of two solid-liquid equilibria is expected, resulting in melanterite ($FeSO_4 \cdot 7\,H_2O$) (see Equation 2.1) and szomolnokite ($FeSO_4 \cdot H_2O$) (see Equation 2.2) as solids [14–18].

The published data from Cameron (1930) and Bullough *et al.* (1952) refer to the solubility limits found at 25°C. Compared, they show similarity in the region of solid-liquid equilibria with melanterite, from 0 wt% to around 27 wt% of H_2SO_4. For higher concentrations of H_2SO_4 the solid-liquid equilibria is with szomolnokite. Cameron (1930) reports the solid phase change at 27.8 wt% H_2SO_4 and 10.7 wt% $FeSO_4$, while Bullough *et. al* (1952) reports it at 30.0 wt% H_2SO_4 and 10.4 wt% $FeSO_4$ [14,15]. Meanwhile, Kobe and Fredrickson (1956) reported their experimental results at 27°C [18]. Despite the slight difference in tem-

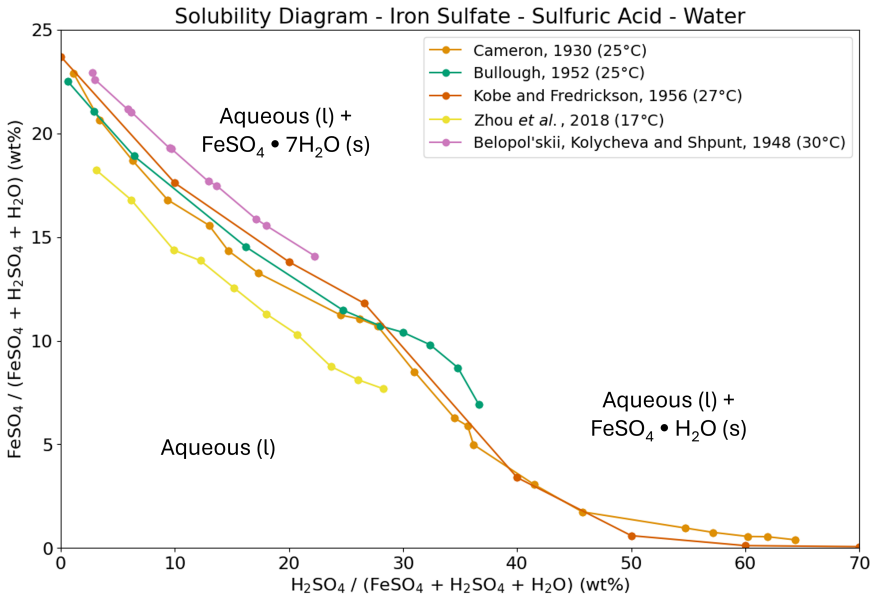

Figure 2.4 Literature data on solubility diagram for iron sulfate - sulfuric acid - water system [14–18]. Circles are experimental data and lines are only included for visual ease.

perature, their results are consistent with the behavior described by the other two authors at 25°C. Kobe and Fredrickson (1956) experimentally found that the transition point from melanterite to szomolnokite occurs at 26.6 wt% H_2SO_4 and 11.8 wt% $FeSO_4$, which is a lower concentration of H_2SO_4 and a higher concentration of $FeSO_4$ [18] when compared to authors at 25°C.

This temperature dependence is also observed when comparing these results with those of authors such as Zhou *et. al*, (2018) at 17°C and Belopol'skii *et. al* (1948) at 30°C [16,17]. At 17°C, it can be seen that the solubility limit is shifted to lower concentrations of $FeSO_4$ [16] and at 30°C, it is observe the opposite behavior, the concentrations of $FeSO_4$ are higher [17], both behaviors in the range of melanterite formation. The same effect was shown for the binary system containing only iron sulfate and water (see section 2.2.2). Through the data presented, it is not possible to clearly identify the impact of temperature on the solid phase change, but all the authors reported different isotherms, and this trend is discussed in their respective papers [14–18].

Table 2.1 summarizes the main aspects of the methodologies used by the authors mentioned in this section. Compared, it can be verified that some sample preparation are similar. Bullough *et al.* (1952), Kobe and Fredrickson (1956) and Cameron (1930) determined the solubility limits based on known compositions of a supersaturated solution of $FeSO_4$, H_2SO_4, and H_2O, under isothermal conditions and constant agitation until solid-liquid equilibrium

was identified. This time varied from 1 to 15 days depending on the authors and temperatures under study. Zhou *et al.* (2018) evaluated the solubility limits through increasing in $FeSO_4$ composition until solid-liquid equilibrium is identified. Belopol'skii *et al.* (1948), on the other hand, obtained the solubility limits of a given solution based on changes in its temperature. To avoid oxidation of the solutions, they all used oxygen-free environments, such as nitrogen or argon [14–18].

Table 2.1: Literature review on methodologies. [14–18]

	Sample preparation	**Range of Temperatures**	**Solution analysis**	**Solid analysis**
Bullough *et. al* (1952)	Supersaturated solutions agitated in a thermostatically controlled bath. The equilibrium was established in a range of 3 to 15 days.	100, 80, 60, 55, 45, 25 and 0°C.	Ferrous sulfate: Titration with potassium dichromate; Sulfuric acid: Precipitation of barium sulfate.	Filtered, washed with alcohol and ether and then analyzed by gravimetry.
Kobe and Fredrickson (1956)	Tubes with solutions connected to a rotating wheel submerged in a constant temperature bath for 24h or more.	0, 27, 40, 60 and 100°C	$FeSO_4$ >1%: Potassium permanganate; $FeSO_4$ <1%: Colorimetric methods; H_2SO_4: Sequester iron with potassium flouride and titrate free acid.	Schreinemakers' method
Cameron (1930)	Supersaturated solutions (30 to 50 grams in 150ml) until equilibrium is reached slowly (a week or more).	0, 25, 55, 65 and 75°C	Fe: Gravimetrically with ferric oxide; SO_4: Precipitation of barium sulfate.	Schreinemakers-Bancroft
Zhou *et al.* (2018)	Solubility: increasing concentration of $FeSO_4$ in acid solutions (H_2SO_4 or H_2SO_4-HCl) Temperature controlled bath. Phase-transition: specific concentrations stirred in thermal equilibrium for 24h.	10, 17 and 35°C	Mass verification	X-Ray Diffraction and Scanning Electron Microscopy
Belopol'skii *et. al* (1948)	Tubes with solutions immersed in Dewark flask containing cooling mixture and analyzed using a visual polythermal method, Alekseev-Bergman.	10, 15, 20, 25, 30, 35, 40 and 45°C	Fe: permanganate; SO_4: Gravimetrically with barium sulfate.	Calculated from the isothermals.

Besides experimental studies, some authors have also reported important information about the $FeSO_4 - H_2SO_4 - H_2O$ system through thermodynamic models [19, 38]. Based on experimental data from some of the authors mentioned above, Charykova *et al.* (2010) focused on modeling the Pitzer parameters for this and other ternary aqueous systems [19]. From their results at 25°C, different physicochemical characteristics could be modeled, such as "[...] *calculations of the activity coefficients of components of the mineral forming solution and the partition coefficients between liquid and solid solutions* [...]" [19]. In this way, Kobylin *et al.* (2007) also modeled the Pitzer parameters at different temperatures (25° to 54°C) [38]. As a result, the authors presented ternary diagrams for this system, highlighting mainly the

impact of temperature on the changes between the two possible phases to be formed from the aqueous solution (melanterite and szomolnokite) [38]. In the model calculated at 25°C, the change from the formation of the heptahydrate phase to the monohydrate phase occurs at around 0.3 mass fraction of H_2SO_4 and 0.1 mass fraction of $FeSO_4$, while at 54°C, the authors report only the presence of the monohydrate phase as a solid phase in the system [38]. This behavior again highlights the influence of the temperature of analysis on the solubility limits of sulfates in aqueous media.

2.3.2 Iron Sulfate - Nickel Sulfate - Water

A second ternary system, containing iron sulfate ($FeSO_4$), nickel sulfate ($NiSO_4$), and water (H_2O), is the subject of study in this work. Different from the previous system, there is limited literature data available about the solubility diagram for this system, despite it being a system of interest due to the presence of these components after the leaching of hydrometallurgical processes [1, 4].

In their article, Charykova *et al.* (2010) present experimental results and parameters from Pitzer's equations. The experimental data were obtained at 20°C and were originally reported by Kogan *et al.* (1970), which we were unable to access due to library limitations [19]. Both experimental and modeled results showed the formation of a solid solution. In other words, they verified the presence of Ni in the melanterite basis ($FeSO_4 \cdot 7\,H_2O$) and Fe in the morenosite basis ($NiSO_4 \cdot 7\,H_2O$) [19]. According to the graph shown in Figure 2.5 and in their work, the transition point from melanterite base to morenosite base at 20°C occurs at molality concentrations of approximately 8.7 wt% $FeSO_4$ and 20.2 wt% $NiSO_4$ [19]. At a temperature of 25°C, the molality concentrations of $FeSO_4$ and $NiSO_4$ are approximately 10.0 wt% and 20.4 wt%, respectively [19]. Thus, as expected, it is possible to visualize the dependence of the solubility of sulfates on temperature, where the higher the temperature, the greater their solubility, even in the presence of a solid solution. As with the ternary system discussed above, this model allows the determination of different physicochemical characteristics of the system.

Other authors have studied the miscibility gap of the solid solution formed by this system. Rutstein (1980) observed the presence of solid solution $(Fe, Ni)SO_4 \cdot 7\,H_2O$ occurring as a result of human activities near the Sudbury mine (Ontario) [44]. Balarew *et al.* (1973) describe that at 20°C, the miscibility gap in the system containing $FeSO_4$ and $NiSO_4$ occurs between 19 and 54 mol% of $FeSO_4 \cdot 7\,H_2O$. Where the basis will be morenosite (orthorhombic) in the concentration range from 0 to 19 mol% and, from 54 mol% on, the base structure will be melanterite (monoclinic) [20]. The article also suggests that when there is a distinction

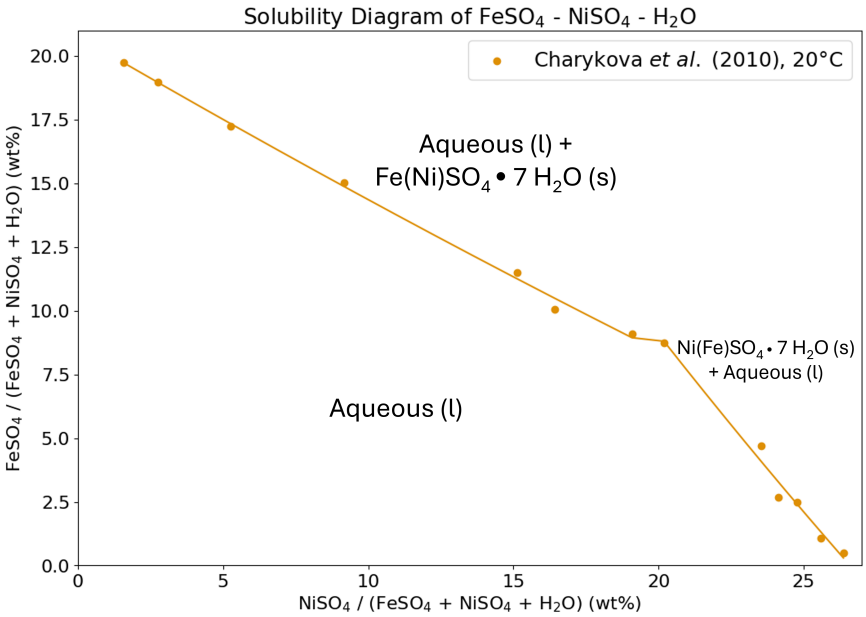

Figure 2.5 Solubility diagram presented by Charykova *et al.* (2010) for the iron sulfate - nickel sulfate - water system. Circles are experimental data and lines are only included for visual ease [19].

between the crystal structures of the end-members, two series of isomorphism are presented, one before and one after the miscibility gap [20].

Equations that describe the thermodynamic solid-liquid equilibria associated with the $FeSO_4$–$NiSO_4$–H_2O system, as well as its particularities such as the presence of solid solution and assumptions, are found in section 5.2.

CHAPTER 3 KNOWLEDGE GAP AND OBJECTIVES

The literature review presented in Chapter 2 discussed the solubility of $FeSO_4$ in different concentrations of H_2SO_4 diluted in water, as analyzed by different authors [14–18]. The generation of data for this system can be used to evaluate the experimental protocol to be extrapolated to those for which little or no literature exists. In addition to the previously mentioned system, the aqueous system containing $FeSO_4$–$NiSO_4$ was discussed. It was noted that, to our knowledge, only one experimental data set has been reported in the literature at 20°C and modeled at 20°C and 25°C, generating the only thermodynamic constants we are aware of [19]. Furthermore, the possibility of solid solution formation was mentioned by Balarew *et al.* (1973), but its further description and description of the solid were not explored by other authors [20]. Therefore, conducting experiments at temperatures other than room temperature may provide new information and insight regarding the description of the solubility and solid solution miscibility gap of this system.

Based on the gaps of knowledge presented, the main objective of this work was to probe the solubility of aqueous systems containing $FeSO_4$–H_2SO_4 and $FeSO_4$–$NiSO_4$ for hydrometallurgical applications, divided into the following specific objectives:

- Experimentally collect solid solution / aqueous solution equilibria data regarding the system $FeSO_4$–$NiSO_4$–H_2O;
- Evaluate the data generated for the system $FeSO_4$–$NiSO_4$–H_2O against equilibria data computed from the literature-derived equilibrium constants;
- Experimentally collect solubility data for the $FeSO_4$–H_2SO_4–H_2O system in equilibrium;
- Evaluate the experimental protocol for the system $FeSO_4$–H_2SO_4–H_2O against the available literature.

CHAPTER 4 MATERIALS AND METHODOLOGY

In order to achieve the objectives proposed by this study, the samples were carefully prepared and analyzed in laboratories located in Montreal (Quebec) at the Polytechnique Montréal. The samples were handled in appropriate locations in order to avoid contamination and health risks. Potential health risks associated with this work include handling acidic solutions, working in low-oxygen environments, and temperature variations ranging from 5°C to 30°C.

This chapter introduces the solubility measurements methodology which will be used in Chapter 5 and 6, further details are provided in sections 5.3.1, 5.3.2 and 5.3.3.

4.1 Experimental Materials

The iron and nickel heptahydrate sulfates, with the respective chemical formulas $FeSO_4 \cdot 7\,H_2O$ and $NiSO_4 \cdot 7\,H_2O$, were used as solutes to obtain the solutions, section 5.3.1 provide more details. To obtain the solutions presented in Chapter 6, the same iron sulfate was used and, in addition to deionized water, in this case, the following sulfuric acid (H_2SO_4), with an Assay Percent Range of 96% (Fisher Chemical) was also used.

4.2 Solution Preparation

The systems studied in this work where $FeSO_4 - NiSO_4 - H_2O$ and $FeSO_4 - H_2SO_4 - H_2O$. To prepare the solutions, a specialized glass cell was used. Further details on its design and operation are presented in Figure 5.1 in Chapter 5.3.2. This procedure consists in adding

Table 4.1 Identification and concentrations of solutions prepared regarding the system $FeSO_4 - H_2SO_4 - H_2O$.

Sample name	**Concentration (wt%)**	
	$FeSO_4$	**H_2SO_4**
F23H1	23.0	1.55
F17H10	17.0	10.7
F13H26	13.0	26.3
F11H27	11.0	27.0
F8H30	8.00	30.9

a known quantity of solute and solvent to the cell, whose temperature is controlled (30°C), as well as the environment to regulate the amount of oxygen during preparation. The time required to completely dissolve the solute was determined by preliminary experiments using an aqueous solution containing 20 wt% $FeSO_4$, which consisted of measuring the chemical composition via AAS at intervals of 1h30, 2h, 3h, and 17h. The time defined in the protocol is 2h, and to ensure that correct dissolution was achieved for all samples, the chemical composition of the initial solution of each of the systems was analyzed using AAS. The solutions containing $FeSO_4 - H_2SO_4 - H_2O$ were then prepared in different concentrations as described in Table 4.1, defined to respect the solubility limits established in the literature, as discussed in section 2.3.1. The sulfuric acid was diluted before the addition of solute. In both systems, it was extremely important to handle the solutions for subsequent characterization steps inside the glove bag, as described in 5.3.2 to ensure that they did not come into contact with oxygen. This is due to the fact that Fe(II) can be oxidized to Fe(III) in the presence of oxygen in the aqueous solution which can precipitate as a hydroxide, changing the color of the solution to brown [45–47]. Studies aim to characterize the kinetics of this reaction under different conditions, mainly in terms of pH and temperature differences. It was found that the lower the pH and temperature of the solution, the slower the oxidation reaction [45–47]. Further details are provided in section 5.3.2.

4.3 Preliminary solubility measurements

In order to identify the liquidus temperature of the aqueous solutions, the equipment DSC (Nexta DSC600, Hitachi), was used. Inside the glove bag, 7.5 µL aliquots were inserted into low-pressure aluminum pans and sealed using an Electrical Sealer (Hitachi). Knowing the mass of the solution in each crucible, they were placed directly in the DSC.

The samples were subjected to heating and cooling cycles between 30°C and -40°C at rates of 10°C/min, 5°C/min, 1°C/min and 0.5°C/min. To ensure temperature stabilization before the start of the heating or cooling cycle, a waiting time of 10 minutes was used. Figure 4.1 *a* shows the results obtained for the sample containing 20 wt% $FeSO_4$. For this composition, the liquidus temperature was expected to be around 20°C, but no signal was identified at or around the expected temperature. These same experimental conditions were used for all solution concentrations presented in this work. More than 100 DSC measurements were done with different imposed parameters, as mentioned before, but no reliable temperature corresponding to the hydrates melting could be identified. The use of DSC to identify the solid-liquid equilibrium was not reliable for the compositions and conditions tested in the present work.

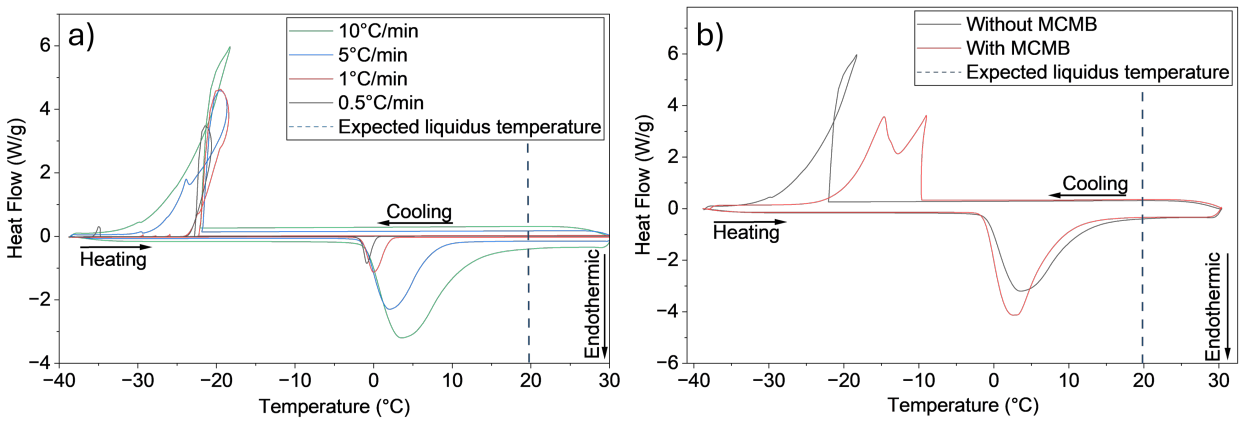

Figure 4.1 Thermograms of the aqueous solution containing 20 wt% $FeSO_4$: a) at different rates; and b) with or without addition of mesocarbon microbeads (MCMB).

Considering that the exposure time of the sample to temperatures below the liquidus temperature was insufficient, new solutions and sealed pans were prepared at the same concentration of 20 wt% FeSO4 and subjected to new cooling and heating cycles. In the new cycles, we tested changing the minimum temperature, reaching -80°C, using slower cooling rates and faster heating rates, waiting times at 5°C of 5 hours and 11 hours, and consecutive cooling cycles to -40°C and heating cycles to 10°C. However, none of them showed reliable results on liquidus temperature identification. In parallel, the addition of nano-inoculants to promote precipitation was also evaluated. Figure 4.1 *b* presents the results obtained with the addition of Mesocarbon Microbeads (MCMB) at a maximum of 3 wt% in the solution containing 20 wt% FeSO4, following the same cycle previously performed at 10°C/min in the temperature range from 30 to -40°C. As a result, the use of MCMB provided better definition in the signal obtained, but was still inconclusive regarding the desired solid-liquid transition. Thus, we followed the hypothesis that the small sample volume submitted to the experiment did not achieve the critical crystal size to initiate precipitation, and then the experimental protocol using 5 mL glass vials was defined.

4.4 Solubility Measurement

Inside the nitrogen-filled glove bag, aliquots of 5 mL were taken from the mother solution and transferred to glass vials. These vials were properly identified, sealed with parafilm, and weighed. Afterwards, the samples were placed in a temperature-controlled chamber (IVYX Scientific) within a temperature range that could include the liquidus temperature of each of the solutions. Every 24 to 72 hours, the temperature was decreased by 2°C and the

samples were inspected for the presence of crystals, in addition to the chemical composition of the liquid being analyzed.

After being filtered, the crystals was subjected to different characterizations, such as chemical (4.4.2), morphological, and structural. All analyses were performed within minutes after filtering in an effort to analyze them before possible dehydration, since the atmosphere couldn't be controlled. Section 5.3.3 provides a description of how the presence of crystals was determined, as well as the steps followed to ensure the correct characterization of the crystals.

The data obtained was analyzed using Profex software were Le Bail refinement methodology was used for the ternary $FeSO_4$–$NiSO_4$–H_2O and Rietveld was used for the ternary $FeSO_4$–H_2SO_4–H_2O. The refinement methods differ in terms of the outputs that can be obtained. In Le Bail's method, only unit cells and peak shapes are refined, without correlating intensities with atomic positions, while Rietveld's use a whole-pattern fitting approach (structural model and peak shapes) to compare the experimental pattern with the calculated pattern [48, 49]. Le Bail technique is known for mainly providing assistance in phase identification when there are peak overlaps [50]. Raiseliene *et al.* (2025) used the same refinement method to evaluate the structure of Mg-WH granules obtained by the dissolution-precipitation method, showing good correlation between the reference and the experimental measurements [48]. Authors as Baek *et al.* (2025) have also used the Le Bail method to confirm the formation of the expected phase ($FeV_3O_9 \cdot nH_2O$) for its subsequent use as a cathode in aqueous Mn batteries [51]. The section 5.3.3 also present details regarding the crystalline structure analysis using XRD technique.

4.4.1 Material Balance

The composition of the liquid can be calculated from mass measurements using the material balance methodology. This chapter will only discuss calculations associated with the system containing sulfuric acid. Descriptions for the binary $FeSO_4$–H_2O and ternary $FeSO_4$–$NiSO_4$–H_2O systems are provided in section 5.3.4. Figure 4.2 illustrates the crystallization process of the ternary $FeSO_4$–H_2SO_4–H_2O system, where the electrolyte liquid is subject to a temperature reduction, which consequently generates the phase separation of a crystalline solid phase and a liquid phase.

In the present system, known masses of $FeSO_4$ (w_{FeSO_4}), H_2O (w_{H_2O}) and H_2SO_4 ($w_{H_2SO_4}$) were initially employed, which represent the composition of the system or equivalently of the liquid solution at temperatures above the liquidus. As the temperature reaches values below the $T_{liquidus}$, a crystal is formed and its mass can be measured ($w^{crystal}_{FeSO_4 \cdot 7\,H_2O}$).

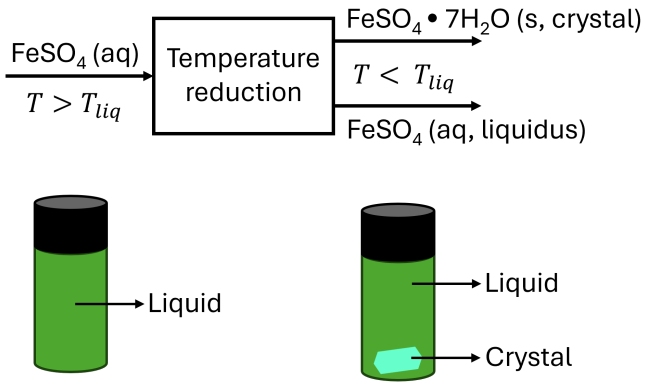

Figure 4.2 Crystallization schematic for a ternary sulfate electrolyte containing $FeSO_4$–H_2SO_4–H_2O.

Assuming the stoichiometry of the crystal is $FeSO_4 \cdot 7\,H_2O$, the following equations can be used to calculate the masses of $FeSO_4$ and H_2O present in the crystal, named as $w^{\text{crystal}}_{\text{FeSO}_4}$ and $w^{\text{crystal}}_{\text{H}_2\text{O}}$ respectively:

$$w^{\text{crystal}}_{\text{FeSO}_4\cdot 7\,\text{H}_2\text{O}} = n^{\text{crystal}}_{\text{FeSO}_4} M_{\text{FeSO}_4} + n^{\text{crystal}}_{\text{H}_2\text{O}} M_{\text{H}_2\text{O}} \tag{4.1}$$

$$7n^{\text{crystal}}_{\text{FeSO}_4} = n^{\text{crystal}}_{\text{H}_2\text{O}} \tag{4.2}$$

In which M_i represents the molar mass and n_i the number of moles of species i, which allows the mass to be calculated using $n_i M_i = w_i$. The weights of the salt and solvents in the liquid solution at the liquidus composition, denoted $w^{\text{liquidus}}_{\text{FeSO}_4}$, $w^{\text{liquidus}}_{\text{H}_2\text{O}}$ and $w^{\text{liquidus}}_{\text{H}_2\text{SO}_4}$ can be resolved via the three following material balance equations:

$$w_{\text{H}_2\text{O}}(T > T_{\text{liquidus}}) = w^{\text{liquidus}}_{\text{H}_2\text{O}} + w^{\text{crystal}}_{\text{H}_2\text{O}} \tag{4.3}$$

$$w_{\text{FeSO}_4}(T > T_{\text{liquidus}}) = w^{\text{liquidus}}_{\text{FeSO}_4} + w^{\text{crystal}}_{\text{FeSO}_4} \tag{4.4}$$

$$w_{\text{H}_2\text{SO}_4}(T > T_{\text{liquidus}}) = w^{\text{liquidus}}_{\text{H}_2\text{SO}_4} \tag{4.5}$$

4.4.2 Chemical characterization (Atomic Absorption Spectroscopy)

Chemical composition analysis was undertaken after crystallization, in order to characterize the saturated liquid solution and the crystal. Once the crystal was formed both the liquid and the crystal present in the vial were separately analyzed. This analysis was performed using AAS, using the same equipment and calibration as described in the section 5.3.5. The first chemical analysis was carried out after crystal formation had been identified in the system $FeSO_4$–H_2SO_4–H_2O. Here, an aliquot of 120 μL was very quickly taken from the liquid solution, which was in contact with the observed crystal in the 5 mL vial after it was removed from the temperature-controlled chamber, to avoid dissolving the crystal formed, and diluted in 12 mL of HNO_3(aq) (3 % volume). A new aliquot of 120 μL was then taken from this new solution and diluted again in 12 mL of HNO_3(aq). The subsequent chemical analysis of the crystal was performed for all systems, following the procedure described in section 5.3.5.

The chemical composition of the liquid present in the system $FeSO_4$–H_2SO_4–H_2O can be calculated from this analysis, where AAS provides the concentration of Fe ($C_{\mathrm{Fe}}^{\mathrm{Diluted}}$) in g/L present in the diluted solution. Therefore, from this result, we can calculate the initial $FeSO_4$ concentration ($C_{\mathrm{FeSO_4}}^{\mathrm{Initial}}$) in g/L of solution (Equation 4.6).

$$C_{Fe}^{\mathrm{Diluted}} \times f^{\mathrm{Initial}} \times \Big(\frac{M_{FeSO4}}{M_{Fe}}\Big) = C_{\mathrm{FeSO_4}}^{\mathrm{Initial}} \tag{4.6}$$

To do this, it is necessary to consider the dilution factor $f = 10000$. Above, the molar mass of Fe (M_{Fe}) and the molar mass of $FeSO_4$ ($M_{\mathrm{FeSO_4}}$) were used. The initial concentration of $FeSO_4$ is then converted to weight percentage ($\phi_{\mathrm{FeSO_4}}$) using the initial concentration of water $C_{\mathrm{H_2O}}^{\mathrm{Initial}}$, which we assume is 1000 g/L.

$$\phi_{\mathrm{FeSO_4}} = \frac{C_{\mathrm{FeSO_4}}^{\mathrm{Initial}}}{C_{\mathrm{H_2O}}^{\mathrm{Initial}} + C_{\mathrm{FeSO_4}}^{\mathrm{Initial}}} \simeq \frac{C_{\mathrm{FeSO_4}}^{\mathrm{Initial}}}{1000\ \mathrm{g/L} + C_{\mathrm{FeSO_4}}^{\mathrm{Initial}}} \tag{4.7}$$

It is important to emphasize that these calculations are an approximation of the concentration of the samples, due to the fact that they do not consider the effect of sulfuric acid in the density of the liquid at T_{liquidus}.

While material balance provides the liquid composition from a known solid composition, AAS allows identification of the liquid composition or the formation of a solid solutions,

and XRD enables the identification of the crystal structure formed to compare it with the structure expected from the literature or a thermodynamic model.

CHAPTER 5 ARTICLE 1: MATERIAL BALANCE PROBING OF AQUEOUS IRON-NICKEL-SULFATE SOLID-LIQUID EQUILIBRIA FROM 6-10°C

Reprinted with permission from Depine Dornelles Da Silva, E., Oishi, K., Harvey, J. P., & Self, J. (2025). Material balance probing of aqueous iron-nickel-sulfate solid-liquid equilibria from 6-10°C. *Journal of Chemical & Engineering Data.* Copyright 2025 American Chemical Society. Submission Date: November 05, 2025.

5.1 Introduction

The motivation for our study of sulfate solutions is the recycling of lithium-ion battery batteries, where one of the main recycling processes is the sulfate hydrometallurgical route. In this process, liquid sulfate aqueous solutions are created as a result of the leaching step with the goal of obtaining selected metal solid sulfate salt hydrates $MSO_4 \cdot nH_2O$ [4]. Here, M is a metal of interest, such as Ni, Co, Mn, Fe or others which can exist in solution as an ion M^{z+}. In many cases, due to a second metal ion N^{z+} in solution, it is difficult to obtain pure salts via chemical precipitation. Such difficulties are compounded by the fact that for many of the sulfate systems, thermodynamic phase equilibria data is unknown or unreported, for example solubilities as a function of temperature at ambient pressure. In fact, high-precision solid-liquid thermodynamic data are of fundamental importance in designing chemical precipitation unit operations to efficiently separate valuable metallic ions from end-of-life Li-ion battery black mass [52]. In this work, we investigate the solubilities of a ternary system of M=Fe and N=Ni ions in solution, noting that practical leachate solutions are often complex with three or more different cations present. We chose this system as an initial case study, in the effort to collect and evaluate previously unavailable solubility data. As far as we know, no phase diagram which includes both solubility limits and tie lines has been reported for this system, motivating our investigation. To allow thermodynamic modelling of tie lines, we report revised solubility constants for iron sulfate in morenosite and nickel sulfate in melanterite. Finally, we note that we experimentally probe solubility limits in a previously unstudied temperature range, from 6 to 10°C.

Ternary transition metal sulfate systems have been the object of both recent and past studies. Many research efforts have focused on metal-acid ternary systems [9, 16, 27]. In such systems, generally, the solid-liquid equilibria are determined by solids of constant composition (also called stoichiometric compounds). In other systems, for example ternary

aqueous sulfates with two different transition metal ions, the solid-liquid equilibria is often determined by solid solutions in which transition metals ions can substitute, at least partially, on given crystallographic sites [36, 42, 53, 54]. However, the aqueous solubility of sulfate solid solutions which hold multiple transition metal ions have been the subject of fairly limited scholarship [19, 53]. In the case of $NiSO_4$ and $FeSO_4$, as far as we know, only Charykova *et al* (2010) [19] have published solubility data and solubility constants of the solid solution. Nonetheless, the biphasic solid compositional region for the solid solution has been previously reported [20, 42, 44]. As is consistent with previous literature, we will refer to the biphasic solid region as a miscibility gap, noting that the two solid phases present in the miscibility gap are comprised of different crystal structures.

5.2 Solid-liquid equilibria

At sufficiently low metal sulfate concentrations, liquid electrolyte/ice equilibrium determines the liquidus via the following equilibrium relation:

$$H_2O\,(s) \rightleftharpoons H_2O\,(l) \tag{5.1}$$

At sufficiently high ionic concentrations, the liquidus is determined by the solubility of hydrates. While studying a temperature window from 0 to 30°C, we assume in this work that the solubility constants of relevance are heptahydrates, [19] such that the two relevant solids are $Fe_xNi_{1-x}SO_4 \cdot 7\,H_2O$ (s,melanterite basis) and $Fe_xNi_{1-x}SO_4 \cdot 7\,H_2O$ (s,morenosite basis). These are solid solutions of iron and nickel sulfates with two different crystal structures, that of the melanterite monoclinic structure and that of the morenosite orthorombic structure. Iron, as part of a melanterite basis, can be described by the following solubility equilibrium:

$$FeSO_4 \cdot 7\,H_2O\,(\text{s,melanterite basis}) \rightleftharpoons Fe^{2+}\,(aq) + {SO_4}^{2-}\,(aq) + 7\,H_2O\,(l) \tag{5.2}$$

Similarly, the solubility of nickel sulfate in the solid solution can also be expressed via a similar equilibrium:

$$NiSO_4 \cdot 7\,H_2O\,(\text{s,melanterite basis}) \rightleftharpoons Ni^{2+}\,(aq) + {SO_4}^{2-}\,(aq) + 7\,H_2O\,(l) \tag{5.3}$$

At sufficiently high nickel sulfate concentrations the solid solution Fy hold a morenosite

basis. The solid-liquid equilibrium with aqueous iron ions and the solid solution can be expressed as:

$$FeSO_4 \cdot 7\,H_2O\,(s,\text{morenosite basis}) \rightleftharpoons Fe^{2+}\,(aq) + {SO_4}^{2-}\,(aq) + 7\,H_2O\,(l) \tag{5.4}$$

Finally, the solid-liquid equilibrium with aqueous nickel ions and this solid solution can be expressed as:

$$NiSO_4 \cdot 7\,H_2O\,(s,\text{morenosite basis}) \rightleftharpoons Ni^{2+}\,(aq) + {SO_4}^{2-}\,(aq) + 7\,H_2O\,(l) \tag{5.5}$$

For equilibria 5.2 and 5.5 the solubility constants have been reported by various groups [19,41,43]. For the nickel in a melanterite basis or iron in a morenosite basis, solubilities at 20 and 25°C have been modelled, and solubilities at 20°C have been reported [19]. However, we were unable to obtain the source publications of the measurements reported in Charykova *et al.* (2010) due to current library limitations. We also note that they do not directly report the composition of the solid solutions as a function of liquid electrolyte composition. At higher temperatures (T > 30°C), it is likely that the solid-liquid equilibria involve other hydrates, as they are part of the known phase diagrams for the corresponding binary systems [8,41,43]. However, we are not aware of any studies considering solid hydrates such as $FeSO_4 \cdot H_2O$ as possible solid solutions.

It is our goal to herein experimentally collect solid solution / aqueous solution equilibria data, and evaluate it against equilibria data computed from the literature-derived equilibrium constants. Using a methodology relying on material balance, we carry out solubility measurements from 6 to 10°C, which we compare to solubility data generated from a thermodynamic model.

5.3 Experimental Procedure

5.3.1 Experimental Materials

In this study, two different sulfates were used to obtain the solutions: iron sulfate heptahydrate $FeSO_4 \cdot 7\,H_2O$, 99.5% pure, purchased from by Thermo Scientific, and nickel sulfate heptahydrate $NiSO_4 \cdot 7\,H_2O$, 99% pure, commercialized by Sigma-Aldrich. The solvent used was deionized water which was obtained using Mili-Q EQ700 water purifier.

5.3.2 Solution Preparation

The liquid electrolyte solutions were prepared in a glass cell (Figure 5.1) inside of a fume hood. The pressure was atmospheric, which is assumed to be the relevant pressure for the present work. The temperature was maintained at 30°C and controlled by a circulating water bath (III) (Lindbergh Blue M, ThermoScientific) and monitored by a thermocouple (IV) (EasyView 11A, Extech). In addition, the cell was connected to a nitrogen bubbler (I) (300 mL/min) and to a magnetic stirrer (350 rpm). Figure 5.1 shows how the cell prevents solution contact with oxygen via pressure difference. All openings were properly closed except for opening II, where there is a tube responsible for transporting excess gases from inside the cell to an aqueous environment. This ensures that no other gases (besides that supplied by the bubbler) can enter and that the pressure will remain constant during the preparation of the solutions.

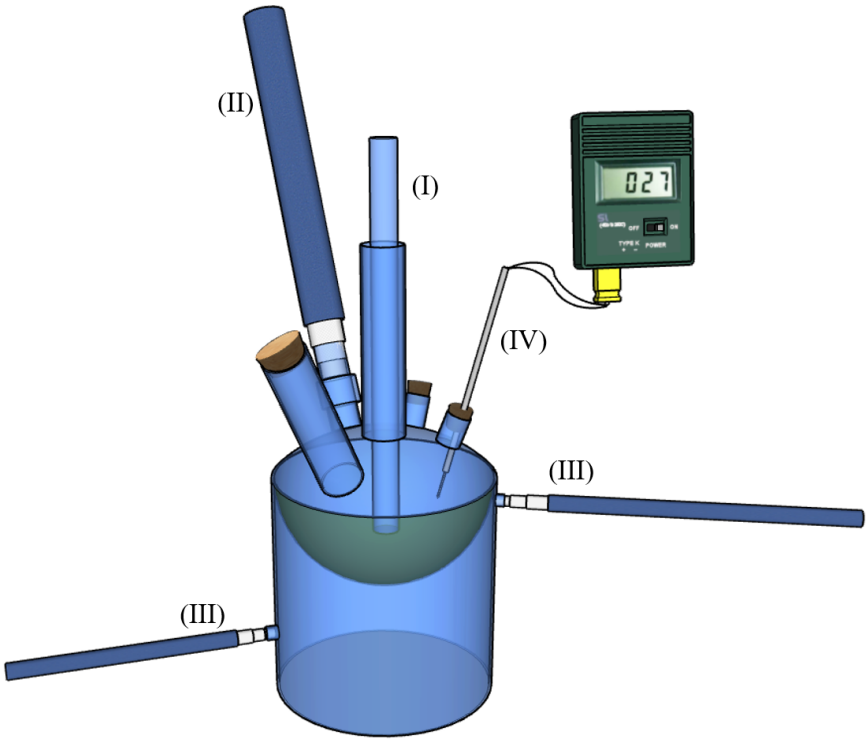

Figure 5.1 Schematic design of the setup used to prepare the solutions. I) refers to the nitrogen bubbler; II) tube for excess gases transportation; III) circulating water bath; and IV) thermocouple.

Firstly, a known concentration of solvent was weighed in a balance (Entris II Sartorius, with accuracy of 0.001 g) and poured into the cell. To ensure a negligible presence of oxygen in addition to temperature homogeneity, the solvent was bubbled while stirring for 40 min. The

solutes were then weighed and introduced into the cell. Stirring and N_2 bubbling were stopped for 5 minutes to allow addition of the solutes, and stirring and bubbling resumed afterwards. After 2 hours, the water bath circulation was stopped, and the solution was transferred to a nitrogen-filled glove bag (Sigma Aldrich) so that the solution could be handled with minimal oxygen concentration (< 2 v%) to the vials where liquid-solid equilibria will be inspected and studied.

5.3.3 Solubility Measurement

The measurement of solubilities of sulfate solutions is in practice somewhat challenging. We first considered using DSC (differential scanning calorimetry) to probe liquidus temperatures. Unfortunately, we were unable to reliably obtain crystallization of the expected solid even with the addition of nano-inoculants to promote precipitation. Following the hypothesis that this is due to the small sample size of the pans (7.5 µL of sample) which prevented the formation of precipitation nuclei of critical size (assuming that nucleation is a stochastic process [55]), we increased the container size by a factor of more than 650 by using 5 mL vials. This allowed formation of crystals in the vials once the temperatures below the liquidus were held for sufficiently long. It is expected that in the concentration ranges studied, the solid-liquid equilibria are determined by transition metal hydrates, which was confirmed via crystallographic analysis. Crystalline structure was analyzed using X-ray diffraction (XRD) (Rigaku, MiniFlex600). In this case, it was necessary to crush the crystals into fine powder using a porcelain mortar and pestle, and then place them in a zero background sample holder. The parameters used consider the XRF (fluorescence X-ray) - reduction energy mode, with an angular range of 3° to 120°, with a step of 0.01° and speed 0.1°/min. The diffraction patterns were analyzed using Le Bail refinement, through the Profex software. Given the difficulty of deconvoluting the XRD signal which holds overlapping contribution from potentially various hydrates, we used the simpler Le Bail refinement over conventional Rietfeld refinement [50]. This allowed identification of the crystal structures present, but not of the exact quantities present, a task which is outside the scope of the current work. The crystals were placed on glass Petri dishes and subjected to morphological analysis using a VHX-7000 optical microscope (Keyence) with lenses ranging from x20 to x80 magnification.

We first prepared the solutions above the liquidus temperature (30°C) and verified visually that all the solution was liquid. To ensure the homogeneity of the solution, the 5 mL of solution were handled using a syringe with a 0.22 µm filter at its tip. Afterwards, we placed the samples in a temperature-controlled chamber at a temperature below the expected

liquidus for 1 day to a week. Following formation of one or many crystals, the vial was weighed before and after the vacuum filtration of the crystals, followed by weighing of the crystals only. Preliminary experiments were conducted to analyze the ratio between the concentration of iron sulfate and nickel sulfate present in the crystals after 1 day, 2 days, 1 week, and 2 weeks of formation. As a result, standard deviations lower than 0.02 wt% were obtained for four different solutions prepared. Provided we have reached thermodynamic equilibrium, and the chemical composition of the crystal is known or estimated, material balance allows calculation of the liquidus composition. A duplicate solution was prepared of the solution above the liquidus temperature containing 5 wt% of iron sulfate and 25 wt% of nickel sulfate, achieving solubilty limits similar to those measured in the first round (within 0.13 wt% for $FeSO_4$ and 0.80 wt% for $NiSO_4$). Accordingly, the measurement of liquidus composition at a given temperature is possible. We describe this general methodology as material balance, noting that it is one of many possible solubility measurement methods [56]. The details of the material balance calculations are in the following subsections. We chose to study solid-liquid equilibria from 6 to 10°C as this allowed the practical study of systems of moderate sulfate concentrations ($\leq$ 25 wt%) through material balance probing, which requires a liquidus temperature sufficiently above the studied temperature for a given concentration.

5.3.4 Material balance

5.3.4.1 Binary material balance

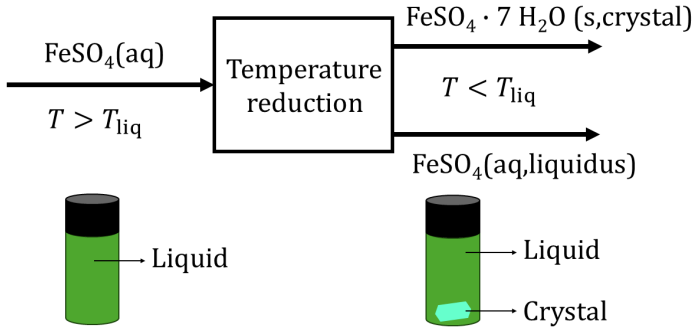

Figure 5.2 Crystallization schematic for a binary sulfate electrolyte.

Figure 5.2 illustrates the crystallization process used in our measurement of solubility for a binary sulfate electrolyte. Specifically, a liquid aqueous electrolyte, once cooled below the liquidus, will separate into a solid crystal phase and a liquid phase of composition equal to that of the liquidus at that temperature. This process, using material balance, allows us to measure the liquidus composition. What is initially known are the masses of H_2O and

$FeSO_4$ in the liquid solution at temperatures higher than the liquidus: w_{H_2O} and w_{FeSO_4}. We note that these are also effectively the system compositions. Once we cool below the liquidus, a crystal is formed with measurable mass $w^{crystal}_{FeSO_4 \cdot 7\,H_2O}$. This mass can be resolved into the masses of H_2O and $FeSO_4$ in the crystal $w^{crystal}_{H_2O}$ and $w^{crystal}_{FeSO_4}$ using the assumed stoichiometry of $FeSO_4 \cdot 7\,H_2O$:

$$w^{crystal}_{FeSO_4 \cdot 7\,H_2O} = n^{crystal}_{FeSO_4} M_{FeSO_4} + n^{crystal}_{H_2O} M_{H_2O} \tag{5.6}$$

$$7 n^{crystal}_{FeSO_4} = n^{crystal}_{H_2O} \tag{5.7}$$

In the above equation, n_i refers to the number of moles of species i , which allows calculation of the mass of the species through $n_i M_i = w_i$ where M_i is the molar mass. The weights of the salt and the water in the liquid solution at the liquidus composition, denoted $w^{liquidus}_{FeSO_4}$ and $w^{liquidus}_{H_2O}$ can be resolved via the two following material balance equations:

$$w_{H_2O}(T > T_{liquidus}) = w^{liquidus}_{H_2O} + w^{crystal}_{H_2O} \tag{5.8}$$

$$w_{FeSO_4}(T > T_{liquidus}) = w^{liquidus}_{FeSO_4} + w^{crystal}_{FeSO_4} \tag{5.9}$$

5.3.4.2 Ternary material balance

The treatment for the binary solution can be generalized for electrolyte systems which are in equilibrium with a nickel-iron sulfate solid solution. Figure 5.3 illustrates crystallization for the ternary iron sulfate - nickel sulfate - water system. In this case, we assume a solid solution is formed in a phase distinct from the liquid aqueous phase for which nickel sulfate and iron sulfate are at the relevant liquidus composition. Equations 5.6 and 5.7 can be generalized to the three following equations, since the solid solution holds both sulfates:

$$w^{crystal}_{Fe_xNi_{1-x}SO_4 \cdot 7\,H_2O} = n^{crystal}_{FeSO_4} M_{FeSO_4} + n^{crystal}_{NiSO_4} M_{NiSO_4} + n^{crystal}_{H_2O} M_{H_2O} \tag{5.10}$$

$$7(n^{crystal}_{FeSO_4} + n^{crystal}_{NiSO_4}) = n^{crystal}_{H_2O} \tag{5.11}$$

$$(1 - x) n^{crystal}_{FeSO_4} = x n^{crystal}_{NiSO_4} \tag{5.12}$$

$x/(1-x)$ is the mole ratio of iron sulfate to nickel sulfate, which can be experimentally resolved if the mass ratio of iron sulfate to nickel sulfate can be measured. In addition to

equations 5.8 and 5.9, there is a material balance equation for nickel sulfate, which allows resolution of the nickel sulfate content at the liquidus composition provided we know the initial nickel sulfate content of the solution above the liquidus temperature and the nickel content in the crystal:

$$w_{\mathrm{NiSO_4}}(T > T_{\mathrm{liquidus}}) = w_{\mathrm{NiSO_4}}^{\mathrm{liquidus}} + w_{\mathrm{NiSO_4}}^{\mathrm{crystal}} \tag{5.13}$$

The equations 5.8 to 5.13 allow resolution of the composition of the liquid in equilibrium with the solid solution provided the masses of the crystal and liquid below the liquidus temperature are measured and the ratio of iron sulfate to nickel sulfate in the solid solution is known. This ratio can be either calculated from a thermochemical model of the solid solution or measured via chemical analysis.

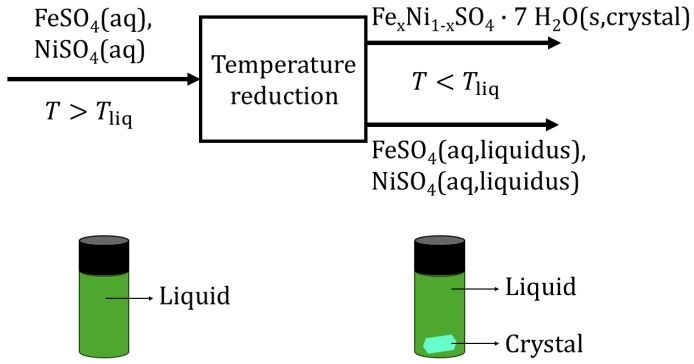

Figure 5.3 Crystallization schematic for a ternary sulfate electrolyte.

5.3.5 Chemical Analysis (Atomic Absorption Spectroscopy)

The chemical composition analysis was performed using atomic absorption spectroscopy (AAS) with a Perkin Elmer Pinaacle 900F spectrometer. According to the calibrations undertaken, Fe measurements within the range of 0 to 2 mg/L have an associated error of 1%, and Ni measurements in the same range have an associated error of 2%. To ensure that all the analyses were within the equipment's measurement range, all the samples were diluted by a volume factor of 10000 using a aqueous solution of 3 v% nitric acid (HNO_3). Two successive dilution steps were used to ensure better dilution accuracy.

Once the crystal formed, the entire crystal present in the vial was dissolved at room temperature in 5 mL of deionized water. To ensure homogeneity of the aliquot analyzed, 1 mL of solution was separated using a syringe with a 0.22 µm pore filter. An aliquot of 120 µL was taken from the filtered liquid solution and diluted in 12 mL of HNO_3. A new

aliquot of 120 µL was then taken from this new solution and diluted again as previously described.

5.4 Model thermodynamics

5.4.1 Solid solution miscibility gap

Table 5.3 shows the solubility constants in logarithmic form for Fe in melanterite and Ni in morenosite, calculated from thermodynamic data provided in Kobylin *et al* (2011) and Kobylin (2011) [41,43]. In order to model the relevant solid solutions, we followed Charykova *et al.*'s (2010) assumption of an ideal Ni and Fe solution in the melanterite ($FeSO_4 \cdot 7\,H_2O$) or morenosite ($NiSO_4 \cdot 7\,H_2O$) host lattices for simplicity [19]. However, we did not use their solid solution solubility constants (see Table 5.3) as these did not adequately reproduce the miscibility gap of the solid solution [42]. The miscibility gap of the morenosite and melanterite structures has been reported as occuring above 0.19 mole fraction Fe content versus Ni in morenosite (i.e. below 0.81 Ni) and below 0.54 Fe content in melanterite (above 0.46 Ni) [42]. In this miscibility gap, L+S_1+S_2 equilibrium involves two solids which are at the fixed composition determined by the miscibility gap and which are at equilibrium. In the case where the energetics in the transition metal solid solutions are approximated as ideal, the solubility constants of the equilibria 5.2, 5.3, 5.4 and 5.5 determine the miscibility gap. Conversely, provided the binary solution solubility constants are known (relevant to equilibria 5.2 and 5.5), the two other solubility constants can be determined if the miscibility gap is known. Since we assume that a thermodynamic equilibrium is established between both solid solutions (i.e. melanterite and morenosite), the following chemical potential equality for the $FeSO_4 \cdot 7\,H_2O$ system component holds:

$$\mu^{\text{melanterite}}_{FeSO_4 \cdot 7\,H_2O}\Big|_{\text{misc. gap}} = \mu^{\text{morenosite}}_{FeSO_4 \cdot 7\,H_2O}\Big|_{\text{misc. gap}} \tag{5.14}$$

The same equilibrium condition also holds for the $NiSO_4 \cdot 7\,H_2O$ system component, specifically:

$$\mu^{\text{morenosite}}_{NiSO_4 \cdot 7\,H_2O}\Big|_{\text{misc. gap}} = \mu^{\text{melanterite}}_{NiSO_4 \cdot 7\,H_2O}\Big|_{\text{misc. gap}} \tag{5.15}$$

Expanding the above equations, we can write the two following equations relating the composition of the structures in the miscibility gap to the various solubility constants, where mel is short for melanterite and mor for morenosite:

$$\ln K_{\mathrm{SP}}(\mathrm{Fe,mel}) + \ln\left(\frac{n_{\mathrm{Fe}}^{\mathrm{mel}}}{n_{\mathrm{Fe}}^{\mathrm{mel}} + n_{\mathrm{Ni}}^{\mathrm{mel}}}\right)\Bigg|_{\text{misc. gap}} = \ln K_{\mathrm{SP}}(\mathrm{Fe,mor}) + \ln\left(\frac{n_{\mathrm{Fe}}^{\mathrm{mor}}}{n_{\mathrm{Fe}}^{\mathrm{mor}} + n_{\mathrm{Ni}}^{\mathrm{mor}}}\right)\Bigg|_{\text{misc. gap}} \tag{5.16}$$

$$\ln K_{\mathrm{SP}}(\mathrm{Ni,mel}) + \ln\left(\frac{n_{\mathrm{Ni}}^{\mathrm{mel}}}{n_{\mathrm{Fe}}^{\mathrm{mel}} + n_{\mathrm{Ni}}^{\mathrm{mel}}}\right)\Bigg|_{\text{misc. gap}} = \ln K_{\mathrm{SP}}(\mathrm{Ni,mor}) + \ln\left(\frac{n_{\mathrm{Ni}}^{\mathrm{mor}}}{n_{\mathrm{Fe}}^{\mathrm{mor}} + n_{\mathrm{Ni}}^{\mathrm{mor}}}\right)\Bigg|_{\text{misc. gap}} \tag{5.17}$$

Following reported miscibility gaps, [42] we solved for $\ln K_{\mathrm{SP}}(\mathrm{Fe,mor})$ and $\ln K_{\mathrm{SP}}(\mathrm{Ni,mel})$ of -4.2155 and -4.4542, as shown in Table 5.3. These values are different from Charykova *et al.* (2010), which, although allow for reasonable modelling of solubility limits, will not reasonably reproduce the miscibility gap.

Since the heat capacities and entropies were not reported for the Ni-Fe solid solutions, [19] we assumed they were invariant for a host lattice for any given iron sulfate-nickel sulfate ratio. This approximation is discussed later on. Table 5.4 and 5.5 show the various employed entropies heat capacities, respectively. This allowed calculation of an enthalpy of formation for the Ni in melanterite and Fe in morenosite, shown in Table 5.4, from the solid solution solubility constants used in the present work (see Table 5.3).

5.4.2 Liquid electrolyte modelling

The binary $NiSO_4$(aq) and $FeSO_4$(aq) electrolytes and their solubilities were modelled following Kobylin *et al.* (2011) and Kobylin (2011) [41,43]. We used their reported enthalpies of formation, entropies and heat capacities for solid compounds and ions in solution, as shown in Table 5.4 and 5.5. For the entropies and formation enthalpies and of heptahydrated iron sulfate in morenosite and and heptahydrated nickel sulfate in melanterite, we used the values in Table 5.4, which were estimated as discussed in the previous section. The water heat capacity parameters were taken from the FactSage database, as shown in Table 5.5 [40]. The nonidealities of the liquid aqueous electrolyte were described using the Pitzer equations. The thermodynamic parameters are shown in the Appendix (Tables 5.5, 5.6, 5.7). In order to model the solubility in the ternary system, we used liquid electrolyte ternary interactions parameters from Charykova *et al.* (2010), which are shown in Table 5.8.

The present work's model was implemented in FactSage, which allowed calculation of the ternary system's phase equilibria [40].

5.5 Results

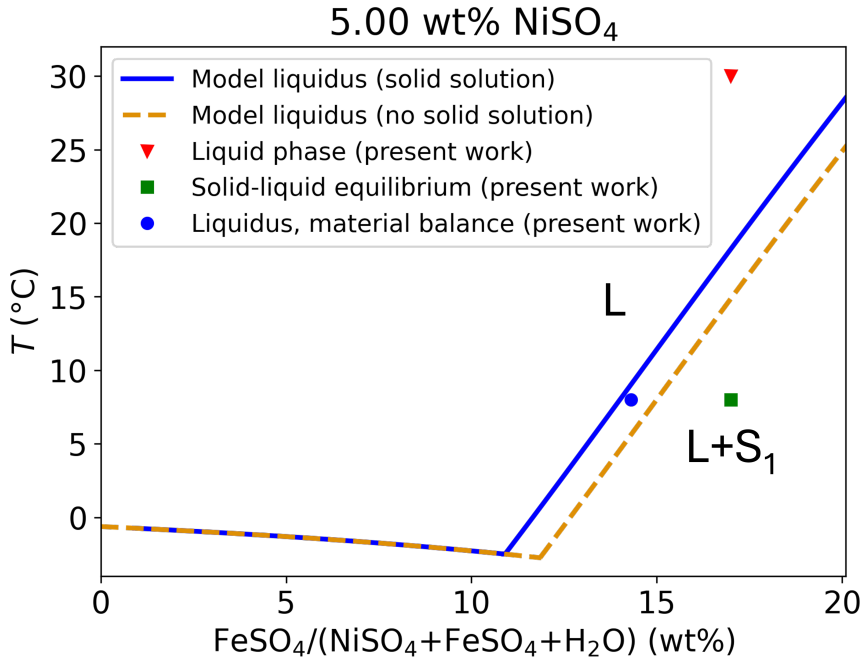

Figure 5.4 Liquidus line along a fixed nickel sulfate weight percent of 5.00%. L means liquidus and S_1 is melanterite.

Figure 5.4 shows the liquidus line for system compositions of 5.00 wt% nickel sulfate computed with the model solid solution (blue) and with the assumption of nickel-free melanterite (dashed line). A solution was prepared at 17.0 wt% $FeSO_4$ and 5.00 wt% $NiSO_4$ at 30°C, which is above the liquidus temperature (red upside down triangle). We cooled the solution vial below the liquidus line to 8°C. After 24 hours, crystals were present, indicating the presence of solid-liquid equilibrium (green square). We note that this is consistent with the solid solution liquidus line shown. Once a crystal is formed, the liquid electrolyte composition changes. Using material balance of a crystal observed for a system of 17.0 wt% of $FeSO_4$ in solid-liquid equilibrium, it was found that that liquid is at a composition of 14.3 wt% $FeSO_4$ in the solution, a quantity resolved using equations 5.8 to 5.13. Such a quantity compares particularly well to the model-computed liquidus composition value of 14.0 wt% at the temperature 8°C. For nickel sulfate, the initial composition is 5.00 wt% and liquidus composition is 4.90 wt% (computed and measured via material balance, see Table 5.1). Generally, since this is a ternary system, the system composition of nickel sulfate will be different than that of the resulting liquidus, and requires special resolution, for example through the use of tie lines.

Table 5.1 Liquidus solution composition ($\frac{w^{\text{liquidus}}_{FeSO_4}}{w^{\text{liquidus}}}$,$\frac{w^{\text{liquidus}}_{NiSO_4}}{w^{\text{liquidus}}}$) at various temperatures as a function of iron and nickel sulfate composition of system ($\frac{w_{FeSO_4}}{w_{\text{Tot}}}$,$\frac{w_{FeSO_4}}{w_{\text{Tot}}}$).

T (°C)	$\frac{w_{FeSO_4}}{w_{\text{Tot}}}$ (wt%)	$\frac{w_{NiSO_4}}{w_{\text{Tot}}}$ (wt%)	$\frac{w^{\text{liquidus}}_{FeSO_4}}{w^{\text{liquidus}}}$ (wt%)	$\frac{w^{\text{liquidus}}_{FeSO_4}}{w^{\text{liquidus}}}$ (wt%)	$\frac{w^{\text{liquidus}}_{NiSO_4}}{w^{\text{liquidus}}}$ (wt%)	$\frac{w^{\text{liquidus}}_{NiSO_4}}{w^{\text{liquidus}}}$ (wt%)
			(mat. bal.)	(model)	(mat. bal.)	(model)
6	20.0	-	16.6	16.1	-	-
8	17.0	5.00	14.3	14.0	4.90	4.90
8	15.0	10.0	12.2	11.2	9.60	9.81
6	11.0	15.0	10.3	8.10	14.6	14.6
8	8.00	18.6	7.70	7.34	17.7	16.7
10	10.0	18.6	8.20	7.39	18.2	17.3
6	1.01	25.0	0.95	0.94	23.7	22.5
6	5.00	25.0	4.90	4.29	23.4	18.9

Figure 5.5 shows the sulfate salt solubilities as a function of total nickel sulfate and iron sulfate weight percentages solid solutions at various temperatures. As for the previously detailed system, the solid-liquid equilibrium was characterized by material balance following the presence of crystals in the liquid vial after a period of one to seven days when its temperature was lowered below the liquidus temperature for each of the samples. For the binary systems (either 0 weight percent $FeSO_4$ or $NiSO_4$), the data from Linke (1958) (squares) [8] shows good agreement with the model data, as expected. The measurements and subsequent material balance (circles), carried out with equations 5.8 to 5.13, show good agreement with the model data. Table 5.1 shows the numerical values of the calculated solubility compositions, denoted as weight percentages $\frac{w^{\text{liquidus}}_{FeSO_4}}{w^{\text{liquidus}}}$ and $\frac{w^{\text{liquidus}}_{NiSO_4}}{w^{\text{liquidus}}}$. One data point, at 23.4 wt% $NiSO_4$ and 4.90 wt% $FeSO_4$, shows noticeable disagreement with the model solubility by 4.50 wt% in nickel sulfate. We note that measuring solubilities often involves scatter, as seen by the Charykova *et al.* (2010) data [19]. The average disagreement for iron or nickel sulfate liquidus compositions are 0.7 wt% and 1.1 wt%, respectively. We thus conclude that the collected data is generally in agreement with the model-predicted solubilities at low temperature.

Table 5.2 Solid solution iron sulfate to nickel sulfate ratio at various temperatures as a function of iron and nickel sulfate composition of system ($\frac{w_{\mathrm{FeSO_4}}}{w_{\mathrm{Tot}}}$,$\frac{w_{\mathrm{FeSO_4}}}{w_{\mathrm{Tot}}}$). The solid phases S_1 (melanterite), S_2 (morenosite) were identified for each system composition, either from XRD or from the model.

T (°C)	$\frac{w_{\mathrm{FeSO_4}}}{w_{\mathrm{Tot}}}$ (wt%)	$\frac{w_{\mathrm{NiSO_4}}}{w_{\mathrm{Tot}}}$ (wt%)	$\frac{\sum_{\mathrm{crystal}} w^{\mathrm{crystal}}_{\mathrm{FeSO_4}}}{\sum_{\mathrm{crystal}} w^{\mathrm{crystal}}_{\mathrm{NiSO_4}}}$ (AAS)	$\frac{\sum_{\mathrm{crystal}} w^{\mathrm{crystal}}_{\mathrm{FeSO_4}}}{\sum_{\mathrm{crystal}} w^{\mathrm{crystal}}_{\mathrm{NiSO_4}}}$ (model)	Phase(s) (XRD)	Phase(s) (model)
6	20.0	-	-	-	S_1	S_1
8	17.0	5.00	7.50	8.77	S_1	S_1
8	15.0	10.0	2.96	3.79	S_1	S_1
6	11.0	15.0	1.11	2.01	S_1, S_2	S_1
8	8.00	18.6	0.35	0.39	S_1, S_2	S_1, S_2
10	10.0	18.6	1.35	1.01	S_1, S_2	S_1, S_2
6	1.01	25.0	0.040	0.031	S_2	S_2
6	5.00	25.0	0.13	0.16	S_2	S_2

Figure 5.6 shows the boundary regions (black line) of different phases present as a function of composition at 8°C. As samples were prepared in the liquid phase and cooled sufficiently to allow solid-liquid equilibrium, a solid phase appeared. The resulting compositions of liquid and solid phases were computed via the model (squares) along with their respective tie lines (dashed line). These compositions were also calculated through experimental material balance measurements (circles), with the corresponding tie lines (dotted line). The measured liquidus compositions agree reasonably well, as described previously for Figure 5.5. Table 5.2 shows the solid solution compositions, measured via material balance or computed from the thermodynamic model. Analyzing the compositions of $FeSO_4$ and $NiSO_4$ from the ratio calculated through AAS and the thermodynamic model, we found an average error of 3 wt%, showing general agreement. The sample that showed the greatest disagreement was in the system at 11.0 wt% $FeSO_4$ and 15.0 wt% $NiSO_4$ with an 8 wt% error for both sulfate compositions. This sample showed considerable disagreement in the solid composition expected from the thermodynamic model — we note that this sample took a week to crystallize while other samples crystallized on the order of 24 hours. Thus we speculate that this is due to kinetic limitations in obtaining the thermodynamically stable phases on the time scales of

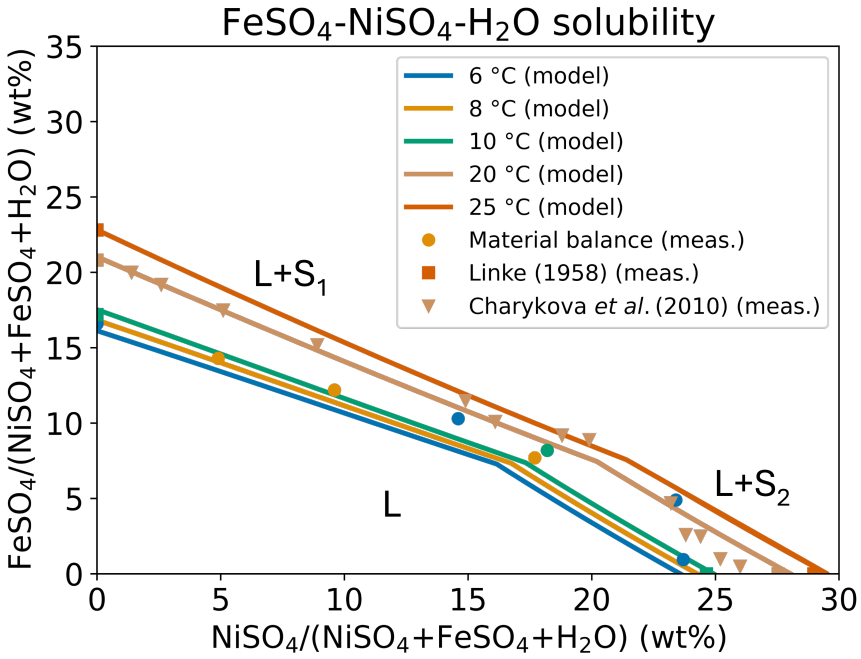

Figure 5.5 Solubilities as a function of total iron sulfate and nickel sulfate weight percentages in the mixture at various temperatures. The labels L denotes liquidus, S_1 melanterite and S_2 morenosite.

the experiment.

Table 5.2 shows the model-predicted solid phases (melanterite S_1, morenosite S_2, $S_1 + S_2$) of the various regions, which are also labelled in Figure 5.6. All measured solid compositions were in the same regions as the model-calculated solid compositions, except for the 11.0 wt% $FeSO_4$ and 15.0 wt% $NiSO_4$ for which the experimental solid composition was in the $S_1 + S_2$ region instead of the S_1 region. We note the liquidus composition of this system was not found to be at the expected value for $L + S_1 + S_2$ systems, which is fixed at a single composition at a single temperature. This is unlike the two other system compositions which are in the model-identified $L + S_1 + S_2$ region, which at 8 and 10°C, showed similar liquidus compositions, with a small difference we associate to the difference in temperature. This agreement suggests that these systems likely reached solid-liquid equilibrum while the 11.0 wt% $FeSO_4$ and 15.0 wt% $NiSO_4$ may not have. Generally, given the agreement of the experimental solubility limits and the tie lines with those calculated from the thermodynamic model, the revised K_{SP} values we suggest for iron in morenosite and nickel in melanterite (see Table 5.3) and their corresponding thermodynamic properties in Table 5.4 are adequate to describe the solid-liquid equilibria from 6 to 25°C. The approximations mentioned above made to estimate the entropy and enthalpy of a given solid solution could be corrected in fur-

ther work by studying the temperature dependence of the solid miscibility gap composition as well as the heat capacity of the solid solutions.

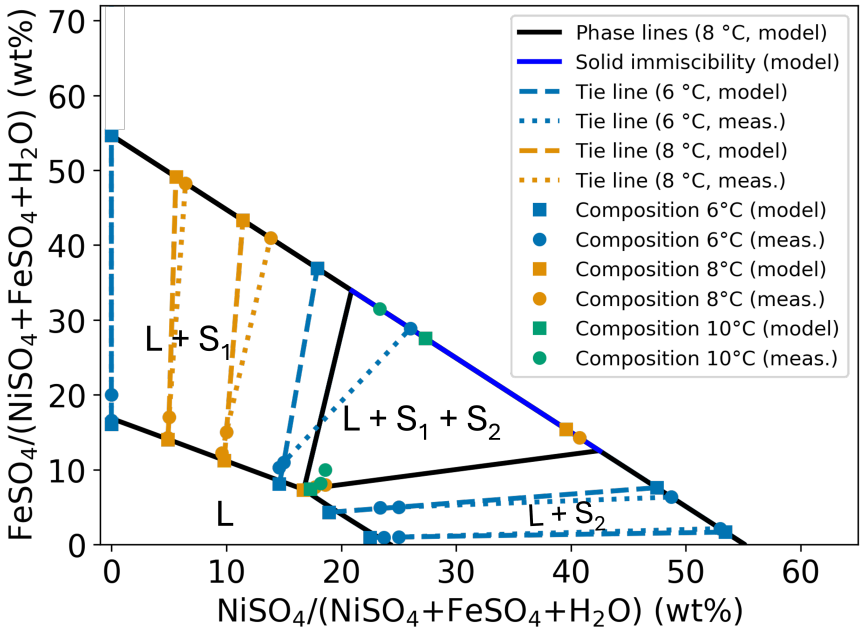

Figure 5.6 Isothermal ternary phase diagram of $FeSO_4$–$NiSO_4$–H_2O. Points computed from the thermodynamic model are shown as squares. Points as circles are computed from material balance and chemical analysis. The identified phases are liquidus L, melanterite (S_1) and morenosite (S_2). Experimental and model-calculated data points in the immiscible region (S_1+S_2) are not indications of miscibility but of the cumulative composition of all solids present (see Table 5.2).

In order to verify that the solids in the different phase regions had the crystallographic structures corresponding to those indicated by the model, crystallographic analysis was undertaken. Figure 5.7 shows diffraction profiles obtained in three different solid formation regions presented above. Given that the XRD sample holder was at room temperature and did not have humidity control, the thermodynamic conditions of the studied solids were not exactly those of the solid-liquid equilibria from which they appeared. As such, they were subject to potential dehydration. The diffractograms showed diffraction patterns implying the presence of phases S_1 and/or S_2, as well as rozenite ($FeSO_4 \cdot 4\,H_2O$) and nickelhexahydrite (β-$NiSO_4 \cdot 6\,H_2O$), but not retgersite (α-$NiSO_4 \cdot 6\,H_2O$). We assume that these lower hydration phases are not the thermodynamically stable phases that would appear in aqueous solid-liquid equilibria at low temperature but exclusively consequences of the dehydration of melanterite and morenosite, respectively. The dehydration of $FeSO_4 \cdot 7\,H_2O$ has been studied by different authors [16, 42, 57, 58], who agree that, under conditions with relative humidity

(RH) less than 55-65% at room temperature (T = 25°C), the heptahydrate structure decomposes into the tetrahydrate structure. The thermodynamic properties of rozenite shown in Table 5.4 are consistent with these dehydration conditions. The dehydration pathway can be described via the following equation:

$$\mathrm{FeSO_4 \cdot 7\,H_2O\ (s)} \xrightarrow[\mathrm{RH \leq 65\%}]{\mathrm{T = 25°C}} \mathrm{FeSO_4 \cdot 4\,H_2O\ (s) + 3\,H_2O\ (l)} \tag{5.18}$$

Furthermore, according to Mitchell (1984) [58], the tetrahydrate structure of rozenite remains stable as long as the above conditions remain unchanged, especially without an increase in temperature to around 40°C. A similar logic applies for the dehydration of morenosite. It reportedly only remains stable at ambient temperature at high RH (>85%), and under sufficiently dry conditions, it dehydrates into beta hexahydrate [59–61]. However, unlike rozenite, nickelhexahydrite does not remain stable, transitioning to retgersite (α-$\mathrm{NiSO_4 \cdot 6\,H_2O}$) after a certain period of time [59–61]. Equations 5.19 and 5.20 summarize these dehydration steps:

$$\mathrm{NiSO_4 \cdot 7\,H_2O\ (s)} \xrightarrow[\mathrm{RH \leq 85\%}]{\mathrm{T = 25°C}} \beta\text{-}\mathrm{NiSO_4 \cdot 6\,H_2O\ (s) + 1\,H_2O\ (l)} \tag{5.19}$$

$$\beta\text{-}\mathrm{NiSO_4 \cdot 6\,H_2O\ (s)} \underset{\mathrm{Time}}{\rightarrow} \alpha\text{-}\mathrm{NiSO_4 \cdot 6\,H_2O\ (s)} \tag{5.20}$$

The thermodynamic properties of nickelhexahydrite and retgersite shown in Table 5.4 [41] are consistent with these dehydration conditions. Although the presence of (Ni,Fe) solid solutions complicates the energetics of equations 5.18, 5.19 and 5.20, we reasonably assume these still apply provided the environment is sufficiently dry. As a result of analyzing the crystal structure through Le Bail refinement of each of the crystals formed, the refinement was validated through a χ^2 value lower than 1.8. Taking into account dehydration, it was possible to identify phase consistency between the model and material balance solid-liquid equilibria. Table 5.2 shows the phases identified via refinement for the various system compositions (denoted XRD). In the system containing 20.0 wt% $\mathrm{FeSO_4}$, the S_1 phase was expected and, as shown in Figure 5.7, the diffraction profiles correspond mainly to this phase, with a few minor peaks corresponding to rozenite. As discussed previously, for the two systems containing 18.6 wt% $\mathrm{NiSO_4}$ with 8.00 wt% or 10.0 wt% $\mathrm{FeSO_4}$, the presence of phases S_1 and S_2 were expected, and the diffratograms indicate the presence of both phases. The signal of the system containing 10.0 wt% $\mathrm{FeSO_4}$ showed some morenosite dehydration, while the system with 8.00 wt% $\mathrm{FeSO_4}$ did not indicate either of the two phases (rozenite or

nickelhexahydrite). Finally, Figure 5.7 presents the system with 5.00 wt% $FeSO_4$ and 25.0 wt% $NiSO_4$ which appears in Figure 5.6 in the region where only the S_2 phase is stable. As expected, only peaks associated with morenosite and the phase resulting from its dehydration, nickelhexahydrite, were identified.

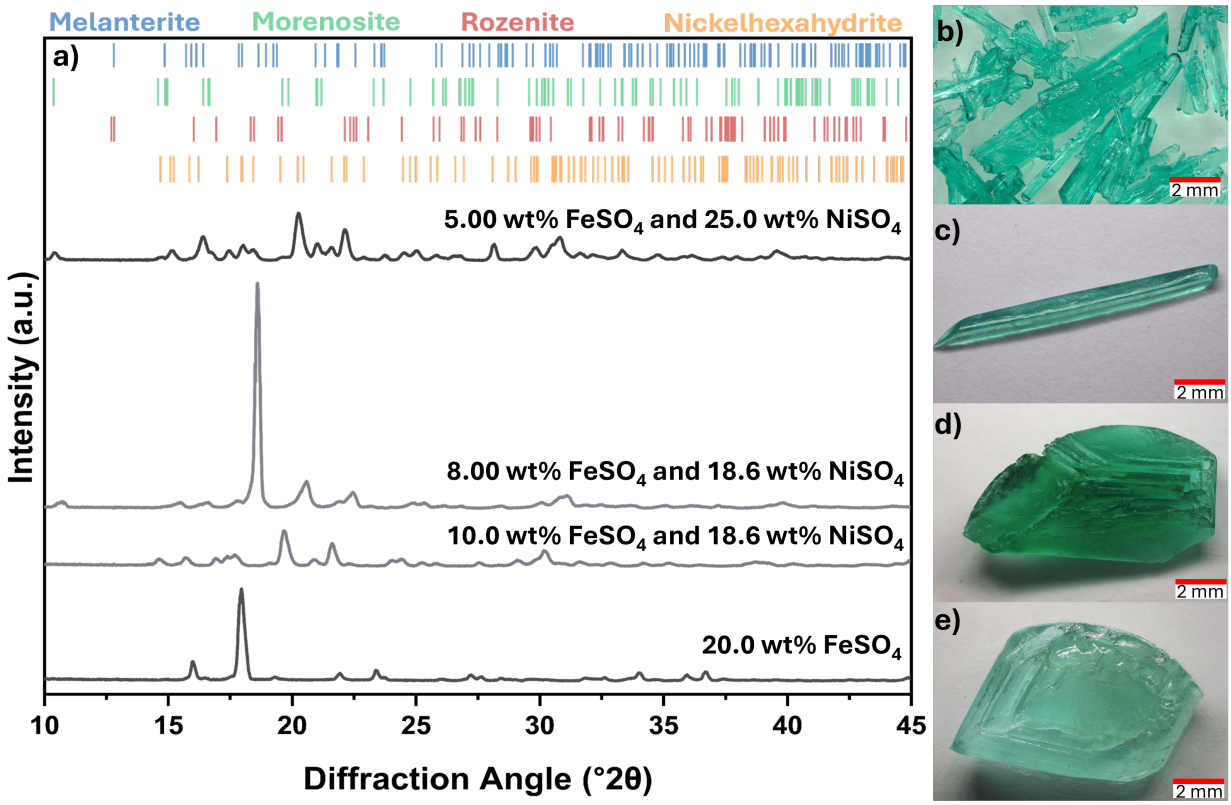

Figure 5.7 a) XRD diffraction pattern of crystals from differents systems. Optical microscope images collected from the experiments; b) 5 wt% $FeSO_4$ and 25 wt% $NiSO_4$, c) 8.00 wt% $FeSO_4$ and 18.6 wt% $NiSO_4$, d) 10.0 wt% $FeSO_4$ and 18.6 wt% $NiSO_4$, and e) 20.0 wt% $FeSO_4$. Scale bar: 2 mm. In this work, we assume the non-heptahydrate forms are results of dehydration occuring during the XRD measurements and are not the thermodynamically stable phases (see text).

Figure 5.7 also presents morphologies corresponding to the diffraction patterns shown. Despite the presence of rozenite and nickelhexahydrite in its patterns, it is expected that the morphology of the crystals will be mainly associated with melanterite, morenosite or a combination these two phases, since dehydration occuring in the present work is not representative of the solid-liquid equilibria under study. Melanterite can be described as a blue-green translucent crystal with a quadrangular prismatic shape [62, 63]. Morenosite, on the other hand, is described as a green needle-like, elongated, or short prismatic crystal [9, 64]. Although the focus of this study was not to determine crystal morphology by considering aspects

such as nucleation, kinetics, and temperature effects, it was possible to observe a correlation between the literature description and the crystals obtained experimentally in this work in regions where the formation of a single phase was expected. In this context, Figure 5.7 *a* and *e* show optical microscope images of the crystals formed in these regions, representing, respectively, the 20.0 wt% iron sulfate system in the melanterite formation region and the 5.00 wt% iron sulfate and 25.0 wt% nickel sulfate system in the morenosite formation region. The two systems containing 18.6 wt% nickel sulfate exhibit morphologies intermediate between the melanterite and morenosite phases. The solid composition of the system containing 10.0 wt% iron sulfate in Figure 5.6 is richer in melanterite, accordingly it exhibits a morphology closer to that observed for the crystal containing only this phase (20 wt% iron sulfate) in *c*. In *d*, the system with 8.00 wt% iron sulfate, whose the solid composition is richer in morenosite, has a morphology more similar to that presented for the crystal containing only this phase (5.00 wt% iron sulfate and 25.0 wt% nickel sulfate).

Figure 5.8 shows the remaining diffraction profiles and their respective morphologies, which also showed peak signals associated with crystal dehydration. In association with Figure 5.6 presented above and the thermodynamic model, the expected phase for systems containing 17.0 wt%, 15.0 wt%, and 11.0 wt% $FeSO_4$ was melanterite, and according to the diffractograms, only the 11.0 wt% $FeSO_4$ and 15.0 wt% $NiSO_4$ system did not agree with the phase predicted from the model. The presence of the morenosite phase in this system is consistent with the experimentally calculated solid composition, where the model predicted only melanterite, but the experiments indicated that when cooled, the solid composition was in $S_1 + S_2$ region. For all three aforementionned compositions, the respective morphologies are accordingly those expected from the XRD-inferred phases, where in *e* and *d* are the systems with 17.0 wt% and 15.0 wt% $FeSO_4$ respectively, they present the quadrangular prismatic shape described for melanterite, and in *c* 11.0 wt% $FeSO_4$, the sample also has a prismatic shape, but with elongated edges, consistent with the description of morenosite [9].

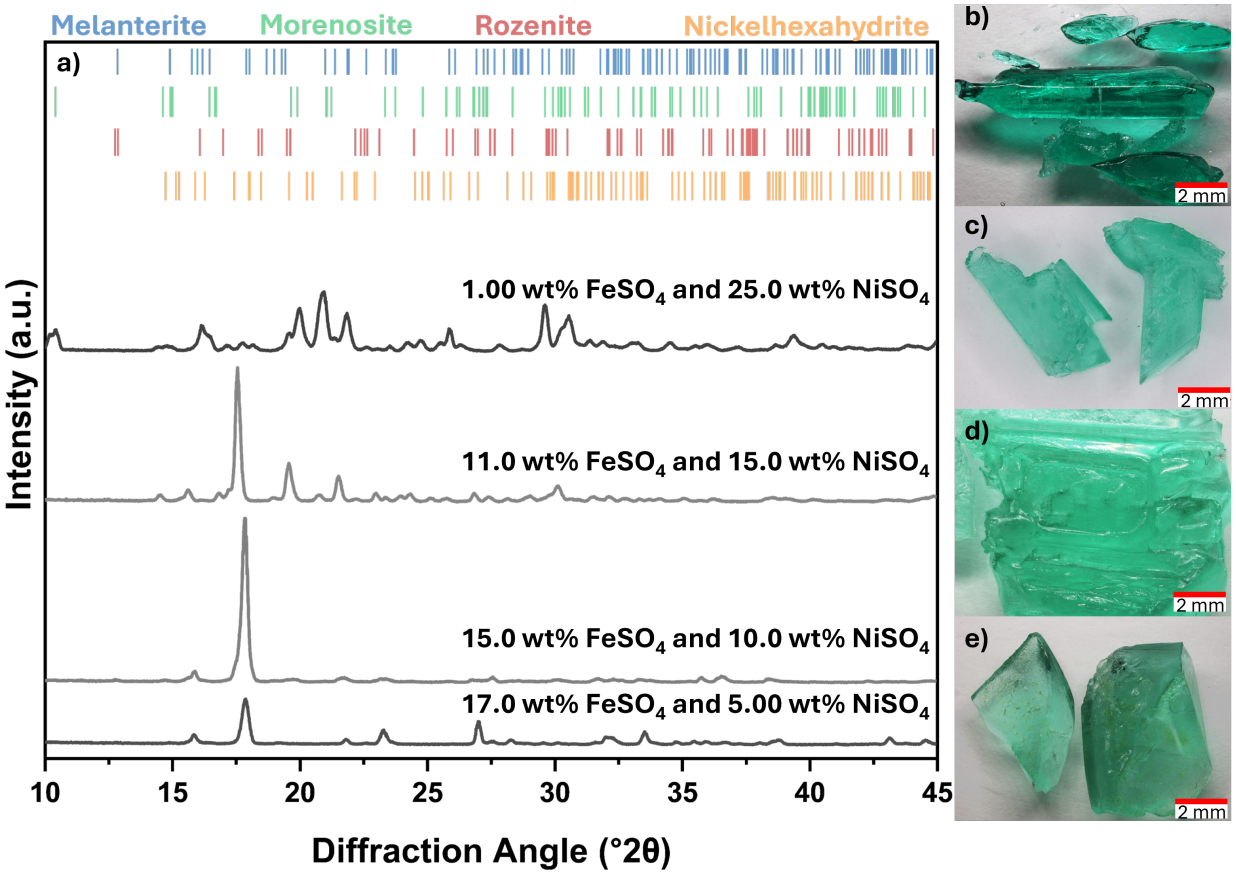

Figure 5.8 a) XRD diffraction pattern of crystals from differents systems. Optical microscope images collected from the experiments; b) 1 wt% $FeSO_4$ and 25 wt% $NiSO_4$, c) 11.0 wt% $FeSO_4$ and 15.0 wt% $NiSO_4$, d) 15.0 wt% $FeSO_4$ and 10.0 wt% $NiSO_4$, and e) 17.0 wt% $FeSO_4$ and 5.00 wt% $NiSO_4$. Scale bar: 1 mm. In this work, we assume the non-heptahydrate forms are results of dehydration occuring during the XRD measurements and are not the thermodynamically stable phases (see text).

5.6 Conclusion

From this work, it was possible to assess the aqueous system of iron and nickel sulfates in terms of solid-liquid equilibria, as well as the presence of solid solutions. The methodology used, which considers cooling the solutions to temperatures below the modeled solid-liquid transition, allowed us to calculate the liquidus composition and solid phases based on the chemical characterization of the crystal through material balance. The collected data were consistent with those computed from the thermodynamic model, where the average disagreement regarding the liquidus composition was on the order of 1 wt% and regarding the solid composition 3 wt% for each of the sulfates. Thus, it was possible to conclude that the experiments and model satisfactorily described the solid-liquid equilibrium. The assumption that

the system would solidify as a solid solution was verified through the crystal composition, found to be consistent with XRD measurement. It is also possible to conclude that the solid solution immiscibility region was adequately described by the thermodynamic model, since the fixed liquid composition of the $L + S_1 + S_2$ region showed agreement for the model and experimental values at two different temperatures, in addition to experimental inference of both solid phases S_1 and S_2. Since data is lacking on the possible solid solution formation of hydrates which are relevant at higher temperatures, we believe their study would be fruitful in the effort to use solid-liquid equilibrium in controlled chemical precipitation and will be subject of future work.

5.7 Appendix 1: Model parameters

Table 5.3 Solubility constants for various solid species, at 25°C.

	$\ln(K_{SP})$	ΔG^0 (kJ/mol)	Reference
$FeSO_4 \cdot 7\,H_2O$ (s,melanterite basis)	-5.2554	13.0279	Kobylin *et al.* 2011
$NiSO_4 \cdot 7\,H_2O$ (s,morenosite basis)	-5.0222	12.4498	Kobylin 2011
$FeSO_4 \cdot 7\,H_2O$ (s,morenosite basis)	-4.2155	10.4500	Present work
$NiSO_4 \cdot 7\,H_2O$ (s,melanterite basis)	-4.4542	11.0418	Present work
$FeSO_4 \cdot 7\,H_2O$ (s,morenosite basis)	-2.35	5.8255	Charykova *et al.* 2010
$NiSO_4 \cdot 7\,H_2O$ (s,melanterite basis)	-3.27	8.1062	Charykova *et al.* 2010

Table 5.4 Thermodynamic quantities used in model.

	ΔH_f^0(298 K) (J/mol)	S^0(298 K) (J/mol · K)	Reference
$FeSO_4 \cdot 7\,H_2O$ (s,melanterite basis)	-3017510.0	395.30	Kobylin *et al.* 2011
$NiSO_4 \cdot 7\,H_2O$ (s,morenosite basis)	-2976610.0	379.16	Kobylin *et al.* 2011
$NiSO_4 \cdot 7\,H_2O$ (s,melanterite basis)	-2970389.8	395.30	See text
$FeSO_4 \cdot 7\,H_2O$ (s,morenosite basis)	-3019744.3	379.16	See text
$FeSO_4 \cdot 4\,H_2O$ (s,rozenite)	-2131060.0	270.60	Kobylin *et al.* 2011
$NiSO_4 \cdot 6\,H_2O$ (s,α-retgersite)	-2683730.0	331.96	Kobylin 2011
$NiSO_4 \cdot 6\,H_2O$ (s,β-hexahydrite)	-2676560.0	353.85	Kobylin 2011
Fe^{2+}(aq)	-92260.0	-105.90	Kobylin *et al.* 2011
Ni^{2+}(aq)	-53973.6	-128.87	Kobylin 2011
$SO_4{}^{2-}$(aq)	-909340.0	18.50	Kobylin *et al.* 2011
H_2O(l)	-285830	69.95	Kobylin *et al.* 2011

Table 5.5 Heat capacities used in thermodynamic model.

	C_P (J/mol·K)	Reference
$FeSO_4 \cdot 7\,H_2O$ (s,melanterite basis)	379.822 + 0.3619T -8224500/T^2	Kobylin *et al.* 2011
$NiSO_4 \cdot 7\,H_2O$ (s,melanterite basis)	379.822 +0.3619T -8224500/T^2	See text
$NiSO_4 \cdot 7\,H_2O$ (s,morenosite basis)	106.688 +0.8655T	Kobylin 2011
$FeSO_4 \cdot 7\,H_2O$ (s,morenosite basis)	106.688 +0.8655T	See text
Fe^{2+}(aq)	14279.4 -57.8948T -258870000/T^2 +0.0659339T^2	Kobylin *et al.* 2011
Ni^{2+}(aq)	16343.1 -66.3614T -296429000/T^2 +0.075689T^2	Kobylin 2011
$SO_4{}^{2-}$(aq)	46200.6 -186.8004T -854629000/T^2 +0.211929T^2	Kobylin *et al.* 2011
H_2O	-203.119+ 1.5207T+ 3848757.662/T^2 -0.0031913T^2 + 0.000002471T^3	FactSage [40]

Table 5.6 Liquid electrolyte binary interaction parameters for $FeSO_4$(aq).

	$FeSO_4$(aq)	Reference
β^0	$-508.3/T + 5.1934 - 0.0161T + 1.8349 \times 10^{-5}T^2$	Kobylin *et al.* 2011
β^1	$-3205.3/T + 15.8514 + 0.0085T - 6.0442 \times 10^{-5}T^2$	Kobylin *et al.* 2011
α	1.4	Kobylin *et al.* 2011
β^2	-16.2142	Kobylin *et al.* 2011
α	12	Kobylin *et al.* 2011
C^ϕ	12.8/T-0.0588	Kobylin *et al.* 2011

Table 5.7 Liquid electrolyte binary interaction parameters for $NiSO_4$(aq).

	$NiSO_4$(aq)	Reference
β^0	-75.73582/T+0.40892	Kobylin 2011 [43]
β^1	-1192.39972/T +7.02089	Kobylin 2011 [43]
α	1.4	Kobylin 2011 [43]
β^2	-79106.27192/T +595.45536 -1.23307T	Kobylin 2011 [43]
α	12	Kobylin 2011 [43]
C^ϕ	41.08029/T -0.09686	Kobylin 2011 [43]

Table 5.8 Liquid electrolyte ternary interaction parameters for $FeSO_4$(aq) + $NiSO_4$(aq).

	$FeSO_4$(aq)+$NiSO_4$(aq)	Reference
$\Psi_{Ni^{2+},Fe^{2+},SO_4{}^{2-}}$	0.05	Charykova *et al.* 2010

CHAPTER 6 COMPLEMENTATY RESULTS: SOLUBILITIES IN $FeSO_4$ – H_2SO_4 – H_2O system

6.1 Results

The Figures 6.1 and 6.2 present the solubilities obtained at 22°C and 6°C, respectively, as a function of $FeSO_4$ and H_2SO_4 concentrations for collected data in addition to existing literature data at similar temperatures [14–18]. In both figures, the blue square represents the experimental values obtained from the calculations presented in equations 4.1 to 4.5 for the material balance methodology, while the blue triangle represents values resulting from the AAS methodology described through equations 4.6 and 4.7. Table 6.1 shows the solubilities calculated by both methodologies for each sample of the system.

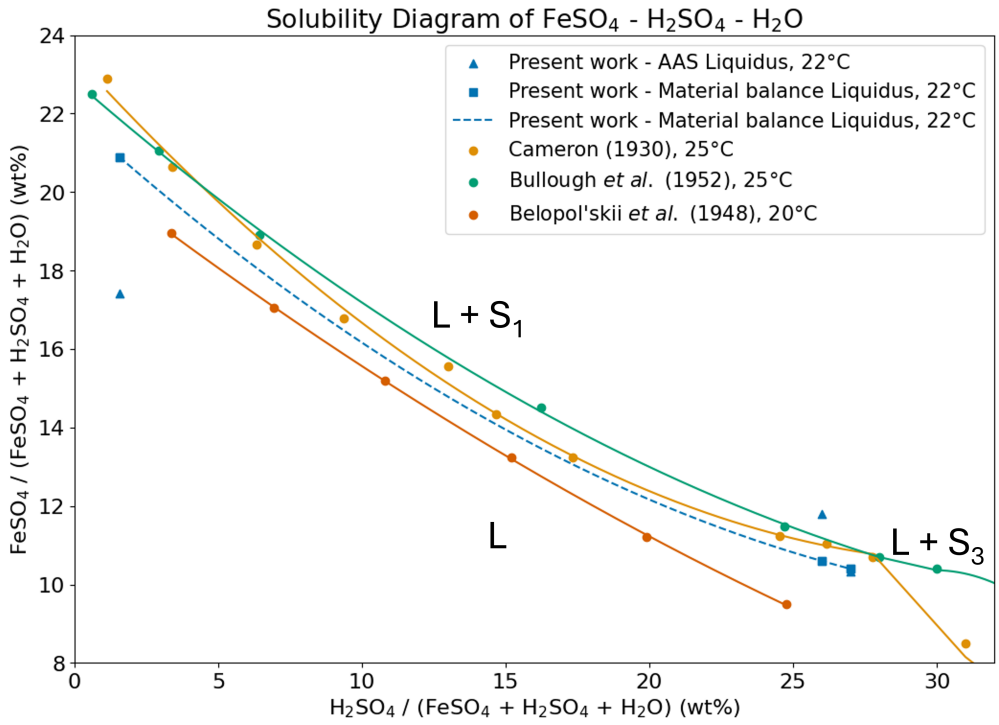

Figure 6.1 Solubility diagram for the $FeSO_4$–H_2SO_4–H_2O system and its comparison with data from various authors at 20°C to 25°C. L represents the liquid phase, S_1 represents melanterite, and S_3 represents szomolnokite. Lines are only included for visual ease. [14,15,17]

Despite variable temperatures, it is possible to compare solubility at 22°C with data at 20°C from Belopol'skii *et al.* (1948) and at 25°C from Bullough *et al.* (1952) and Cameron (1930) [14, 15, 17]. The solubility computed using the material balance for different solutions

at this temperature shows an excellent agreement, as they are close to the reported data at 25°C. Following this same tendency, the solubility computed using AAS for the sample F11H27 also shows good agreement with the data from the literature and the solubility calculated using the material balance. The disagreement between the two methodologies studied in this work was 0.06 wt% for sample F11H27. From the AAS methodology for the liquidus composition of the other samples (F23H1 and F13H26), there is a larger disagreement with reported values from literature. The disagreement between the two methodologies is on average 2 wt% at 22°C, whose respective liquidus composition values are shown in Table 6.1.

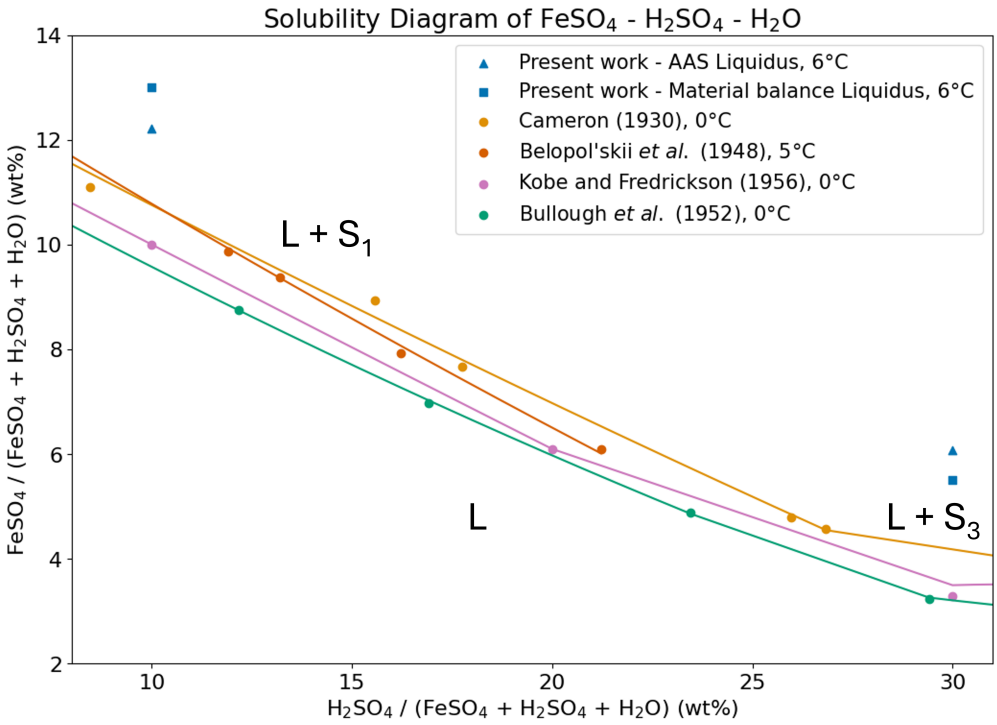

Figure 6.2 Solubility diagram for the $FeSO_4$–H_2SO_4–H_2O system and its comparison with data from various authors at around 6°C. L represents the liquid phase, S_1 represents melanterite, and S_3 represents szomolnokite. Lines are only included for visual ease. [14, 15, 17, 18]

At 6°C no data were found in the literature describing the solubility of $FeSO_4$ in different concentrations of H_2SO_4. However, authors as Cameron (1930), Kobe and Fredrickson (1956) and Bullough *et al.* reported the solubility at 0°C, and Bellopol'skii *et al.* (1948) reported it at 5°C [14, 15, 17, 18]. The data in Figures 6.1 and 6.2 indicate that in these temperature and concentration ranges, solubility generally increases with temperature. The liquidus compositions calculated by AAS and material balance at 6°C, as shown in Figure 6.2, were consistent with the data from the literature presented as both are reported at mod-

erately higher $FeSO_4$ concentration than the lower temperatures [14,15,17,18]. Furthermore, the liquidus compositions calculated in this study for samples F17H10 and F8H30 show an average disagreement between the methodologies of 1 wt%, as can be seen in Table 6.1.

Table 6.1 Liquidus composition at various temperatures $FeSO_4-H_2SO_4-H_2O$. The solid phases S_1 (melanterite) and S_3 (szomolnokite) were identified for each system composition, either from XRD or expected from the literature [15–18, 28].

Sample name	**T (°C)**	**Liquidus composition ($FeSO_4$ wt%)**		**Phase(s)**	**Phase(s)**
		Material Balance	**AAS**	**Expected**	**XRD**
F23H1	22	20.93	17.41	S_1	S_1
F17H10	6	12.96	12.21	S_1	S_1
F13H26	22	10.59	11.79	S_1, S_3	S_1, S_3
F11H27	22	10.39	10.33	S_1, S_3	S_1, S_3
F8H30	6	5.53	6.07	S_3	S_1, S_3

As shown in Figures 6.1 and 6.2, two crystal structures are reported for the concentrations proposed in this study: melanterite ($FeSO_4 \cdot 7\,H_2O$) and szomolonokite ($FeSO_4 \cdot H_2O$), labelled in this work as S_1 and S_3, respectively. Based on their positions in the respective figures and from the literature, it was expected that both samples F23H1 and F17H10 at the studied temperatures would have reach solid-liquid equilibrium with melanterite (S_1) [15–18, 28]. For samples whose concentration of H_2SO_4 is around 26 to 27 wt% (F13H26 and F11H27), it is expected that the solid-liquid equilibrium would be reached in the transition point between the heptahydrate (S_1) and monohydrate (S_3) phases [15, 18, 38]. Finally, for sample F8H30, the presence of the monohydrate (S_3) structure is mainly expected [15,18,28]. This is summarized in Table 6.1.

As for the crystals formed from solutions of the $FeSO_4-NiSO_4-H_2O$ ternary system, it was also possible to identify during analysis of the diffraction profiles the presence of the tetrahydrate structure ($FeSO_4 \cdot 4\,H_2O$), rozenite (see Chapter 5, section 5.5). During the handling of the crystal, which was part of preparing the sample for its characterization, dehydration may have occurred due to the uncontrolled humidity levels in the atmosphere surrounding the XRD analyzes at room temperature. In studies as Zhou *et al.* (2018), the same behavior was reported for samples that should have a heptahydrate crystal structure [16]. This dehydration was also observed when the crystals were manipulated for morphological observation, which occurred without humidity control and at 25°C, as the XRD measurements. Figure 6.3 illustrates the F11H27 crystal, which within a few minutes exhibited indications of the crystal dehydration process. In Figure 6.3 *b*, it is possible to observe the

formation of an opaque white region with possible radial growth. This observation potentially corresponds to the presence of rozenite, whose appearance is described by Anthony *et al.* (2005) as "*cottonball-like concretions and nodules [...] or coatings on melanterite.*" [65]. It is important to note that this behavior was observed in all samples of the $FeSO_4 - H_2SO_4 - H_2O$ system, but with greater intensity in those with higher melanterite concentrations.

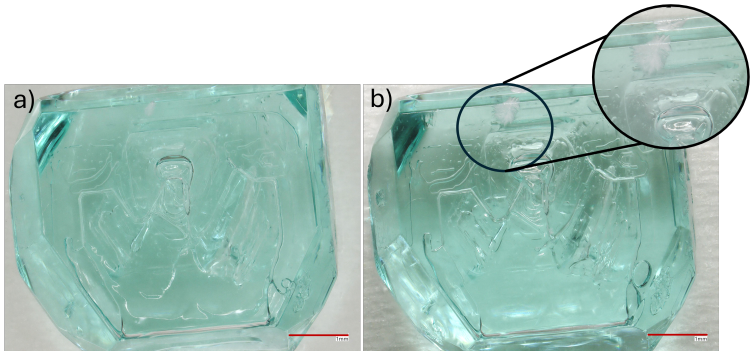

Figure 6.3 Optical microscope image which present indications of the appearance of rozenite in b) when compared to the initial condition in a). Scale bar: 1 mm.

Figure 6.4 *a* shows a comparison between the diffraction profiles of samples F23H1 and F17H10. Qualitative analysis shows that the angles associated with the structure of iron sulfate tetrahydrate coincide adequately with those presented by the samples. After analysis using Rietveld refinement and despite the different temperatures at which the F23H1 and F17H10 crystals were extracted, 22 °C and 6 °C, respectively, it was possible to identify that 100% of the peaks presented by both samples are consistent with rozenite. This is compatible with the expected phase (see Table 6.1), since dehydration is a process that occurs after the crystal is removed from its thermodynamic equilibrium state. Table 6.2 shows the phases obtained for all samples.

Figure 6.5 *a* shows the diffraction profiles of samples F11H27, F13H26, and F8H30. In the diffraction profiles for these samples, the presence of rozenite and szomolnokite was identified. The appearance of both phases is consistent with that presented in Figures 6.1 and 6.2 above and in the Table 6.1, for the samples F11H27 and F13H26 where the solid-liquid equilibrium was achieved at 22°C. The same equilibrium was achieved by the sample F8H30 at 6°C where, according to Table 6.1, only the identification of the S_3 phase was predicted, but it was experimentally determined that rozenite is also present. It is assumed that the presence of rozenite comes from the dehydration of a portion of the heptahydrate phase remaining from the solid-liquid equilibrium, due to the fact that the transition from szomolnokite to rozenite is not favorable under the experimental conditions mentioned earlier. This remaining content may be associated with the influence of temperature on solubility curves. The influence of

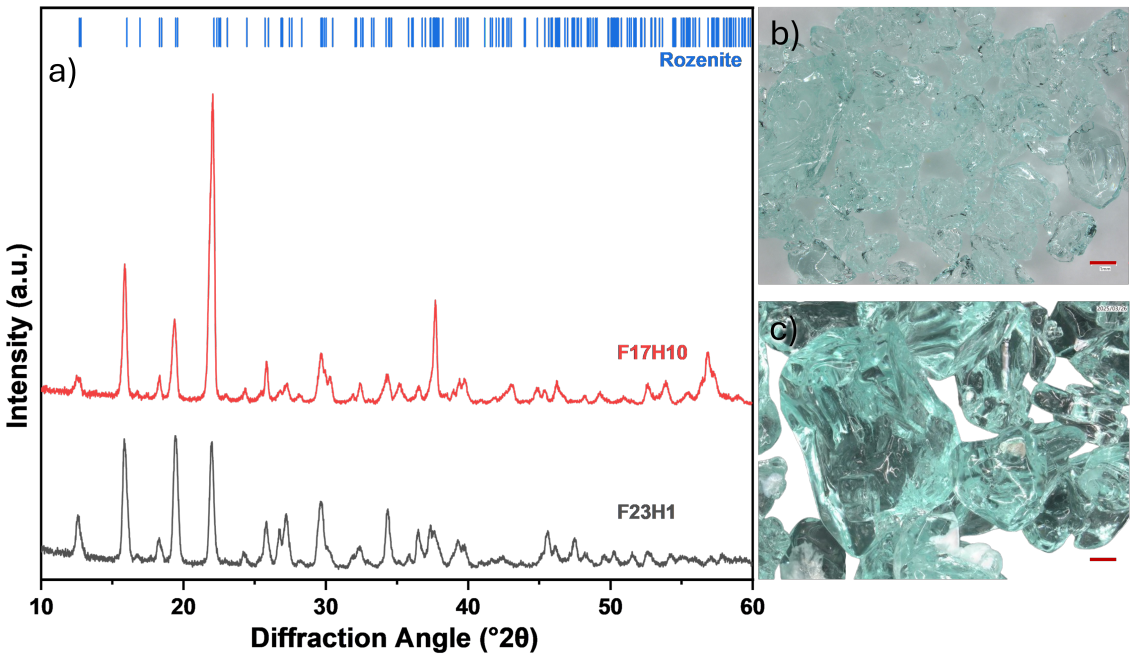

Figure 6.4 Comparison of diffraction patterns of samples containing only rozenite in a). Optical microscope images of the crystal from b) F17H10 and c) F23H1 samples. Scale bar: 1 mm.

temperature becomes clearer when, after Rietveld refinement, the percentages presented in Table 6.2 indicate a higher fraction of szomolnokite for sample F8H30 (90%), where the transition point from the heptahydrate to the monohydrate structure occurs at lower $FeSO_4$ and higher H_2SO_4 compositions than those presented at 22 °C.

Table 6.2: Crystal phase structure for the $FeSO_4 - H_2SO_4 - H_2O$ system.

Sample name	**Phase structure**	**%**	**Phase structure**	**%**
F23H1	Rozenite	100	-	-
F17H10	Rozenite	100	-	-
F11H27	Szomolonokite	55	Rozenite	45
F13H26	Szomolonokite	84	Rozenite	16
F8H30	Szomolonokite	90	Rozenite	10

Optical microscope images of each crystal formed were obtained and are presented in letters *b* to *d* in Figures 6.4 and 6.5. According to España and Ercilla (2008), melanterite in mines can have different characteristics depending on the conditions to which iron sulfate is

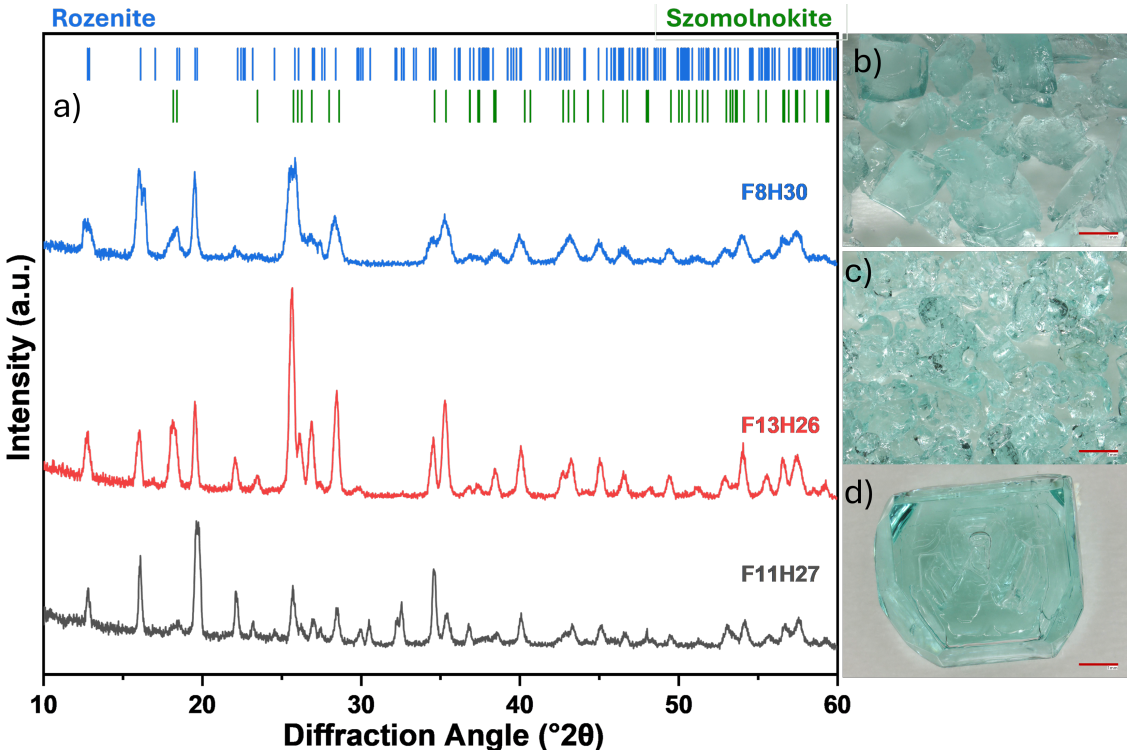

Figure 6.5 Comparison of diffraction patterns of samples containing rozenite and szomolonokite in a). Optical microscope images of the crystal from b) F8H30, c) F13H26, and d) F11H27 samples. Scale bar: 1 mm.

exposed [62]. In their work, they show that under conditions of acidic water accumulation, the crystals formed have a translucent quadrangular prismatic shape. Gomes *et al.* (2017) used the description of "*[...] green, vitrious, prismatic crystals of melanterite.*" [63]. Ulloa *et al.* (2018) described the coloration of melanterite and szomolnokite as green and light blue [66]. The morphology of skomolnokite was described by Wiese *et al.* (1987) as euhedral crystals [67].

The morphology of the crystals, where only the presence of melanterite was expected, is shown in Figure 6.4, where *b* is F17H10 and *c* is F23H1. The image shows that the crystals are very similar in color, which can be described as blue-green, consistent with that described in the literature for iron sulfate heptahydrate. In addition, it is possible to note that there is a certain degree of translucency in the crystals [42, 63, 65, 66]. Furthermore, the shape and size of the crystals changed between F17H10 and F23H1. The sample F23H1 presented a quadrangular prismatic characteristic, with different growth boundaries, making its edges slightly rounded. In terms of shape, sample F17H10 (formed at 6°C) is similar to F23H1, but exhibited a smaller average crystal size than those formed at 22°C.

Crystals whose existing phases were associated with the presence of S_1 and S_3 are shown in Figure 6.5, where *b* is F8H30, *c* is F13H26, and *d* is F11H27. As for the crystals previously discussed, the crystals are similar in blue/green color. However, an increase in the opacity of sample F8H30 can be observed compared to the others. This behavior may be related to the greater presence of the monohydrate phase in the sample. Sample F8H30 has noticeables faces. As for F13H26, it is possible to say that this crystal had a shape similar to the sample described above, but smaller and rounded edges. Sample F11H27, on the other hand, shows a shape comparable to the monohydrate phase, with well-defined faces and no major signs of interference from the nucleation of other crystals.

It can be seen that the morphology shown is consistent with that described in the literature for each of the phases formed, making it possible to correlate the presence of the heptahydrate phase (melanterite) or the monohydrate phase (szomolnokite) with the results XRD results. In addition, the effects of temperature are perceptible in the morphology due to their influence on the solubility diagram of $FeSO_4$ in H_2SO_4. This fact is evident by the presence of szomolnokite being more evident in sample F11H27, whose chemical composition of the starting solution is in the transition point between melanterite and szomolnokite. With decreasing temperature, this transition shifts to higher concentrations of H_2SO_4, and thus sample F8H30 already shows a strong presence of szomolnokite, but still with traces of melanterite among its crystals [14]. Despite these statements, this work does not aim to better identify crystal morphology, such as nucleation studies, formation kinetics, or temperature influences.

CHAPTER 7 GENERAL DISCUSSION

In the literature review (section 2), several aspects were covered that had an influence on the methodology and the results obtained in this study, both in relation to the ternary system $FeSO_4 - NiSO_4 - H_2O$ and $FeSO_4 - H_2SO_4 - H_2O$. Among these aspects, we can mention as the main ones the formation or non-formation of solid solutions, the lack of information available in the literature regarding the existence of miscibility gaps, and the complexity of analyzing the results.

One of the most evident differences between the two systems studied was the possibility of a solid solution formation from the prepared solutions. The formation of solid solution with iron sulfate was observed for the system containing nickel sulfate and not sulfuric acid. This can be rationalized through the chemical similarities between Fe and Ni versus H. Fe and Ni can substitute each other in the solid solution to appreciable extent in melanterite and morenosite. During substitution, the other species (H_2O and $SO_4{}^{-2}$) remain fixed in the lattice, allowing the presence of Fe in the morenosite ($NiSO_4 \cdot 7\,H_2O$) structure and Ni in the melanterite ($FeSO_4 \cdot 7\,H_2O$) structure, depending on the composition. In the case of a system containing sulfuric acid, this third component does not participate in the composition of the solid once solid-liquid equilibrium with the aqueous solution. This promotes exclusive formation of solids with constant composition, in other words, the solid will always have the same composition when the ratio by mass of elements present is fixed [32, 33].

As a consequence of the formation of a solid solution, our results led to the identification and characterization of a miscibility gap region in the $FeSO_4 - NiSO_4 - H_2O$ system, as discussed in Chapter 5. In addition to the lack of extensive information associated with the solubility of this system, only one other study has explored the topic of immiscibility of this system as far as we know [20]. Limited information on immiscibility gaps of other similar systems can also be found [42]. Generally speaking, the solid-liquid equilibria of transition metal aqueous sulfate solutions warrants further investigation. It was found that the published literature is limited in prescribing methodology to study solid solutions in such systems, despite the need for full description of the phase behaviour.

Part of the authors who reported their methodologies for determining the solubility of the $FeSO_4 - H_2SO_4 - H_2O$ system obtained the solid-liquid thermodynamic equilibrium from supersaturated solutions subjected to temperature reduction, either static or under agitation. This method of obtaining the solid phase was used in this study not only for the ternary system containing sulfuric acid, but also for the $FeSO_4 - NiSO_4 - H_2O$ system. The last one

worked adequately, even though the methodology used to obtain the only experimental data we know of was not found.

Each of the ternary systems studied resulted in different approaches to analyze the liquidus composition and phase present in the solid formed due to their particularities discussed above. The liquidus composition of the $FeSO_4 - H_2SO_4 - H_2O$ system covered in this work was analyzed and discussed in Chapter 6 using the AAS methodology (see 4.4.2) and material balance (see 4.4.1). The average disagreement between the two methodologies being 2 wt%, considering both temperatures studied (22°C and 6°C), suggesting that both AAS and material balance could be used to study solid-liquid equilibria. However, the AAS measurement requires volumetric measurements or assumptions not needed in material balance, which may allow this technique to be more flexible when accuracy is needed and volumetric data is unavailable.

The liquidus compositions computed through the material balance agreed more closely with those available in the literature. This could be associated with the assumption used in the AAS calculations, in which the influence of sulfuric acid was not considered. For this reason, the $FeSO_4 - NiSO_4 - H_2O$ system did not include the discussion of its results using this methodology, given that the material balance presented a greater ability to describe the system. Another distinction between the results analysis of the ternary systems was the use of the Rietveld refinement method for the one containing sulfuric acid and the Le Bail refinement for the one containing nickel sulfate. This distinction was based on the difficulty of identifying phases in the $FeSO_4 - NiSO_4 - H_2O$ system due to the large number of overlapping peaks between two phases (melanterite and morenosite), for which LeBail allowed resolution of the underlying features in the diffraction measurement, in agreement with the thermodynamic model. Le Bail does not treat intensities of peaks but only their position in terms of the diffraction angle [48,50]. As such, I propose that Le Bail's refinement can be a useful alternative to Rietfeld refinement when diffraction peak resolution becomes otherwise difficult [48–51].

CHAPTER 8 CONCLUSION

Hydrometallurgical processes are extensively used during LIB recycling, motivating the investigation of aqueous solution containing metal sulfates [2, 3]. However, there is lack of information on how to obtain pure metals from the waste, constituting a serious obstacle [2]. Research is being conducted with the aim of covering this gap by providing a more detailed description of the precipitation and crystallization of the components present in hydrometallurgical residues [4].

In this context, the present work aimed to establish an experimental protocol for solubility measurement based on data collection from the system $FeSO_4 - H_2SO_4 - H_2O$ and its comparison with data from the literature. For this purpose, solutions were prepared and submitted to temperatures below the $T_{liquidus}$ previously characterized in the literature. The liquidus composition was chemically analyzed using AAS and material balance, the structure of the crystals formed was analyzed using XRD and refined using Rietveld. Based on the results, the methodology was implemented for the system $FeSO_4 - NiSO_4 - H_2O$, given the limited literature solubility available for this system. The liquidus composition was in this work analyzed through material balance and compared with a thermodynamic model based on solubility constants previously reported by Charykova *et al.*, (2010) [19]. The crystal was chemically characterized using AAS, and its structure was identified using XRD and Le Bail refinement.

8.1 Summary of Works

- The liquidus compositions from the different solutions prepared for the system containing $FeSO_4 - H_2SO_4 - H_2O$ were calculated using AAS and material balance at 22°C and 6°C. As a result, for both temperatures, consistency was demonstrated when comparing the data obtained through material balance with data from AAS. In other words, the resulting concentrations of $FeSO_4$ at $T_{liquidus}$ presented values within the expected ranges according to the literature data. Despite this, the material balance methodology was incorporated into the experimental protocol used for the system $FeSO_4 - NiSO_4 - H_2O$ because it is more flexible and does not require assumptions related to volumetric solution properties.

- The identification of melanterite ($FeSO_4 \cdot 7\,H_2O$) dehydration was determined through XRD analysis and Rietveld refinement in the $FeSO_4 - H_2SO_4 - H_2O$ system, where traces

of rozenite ($FeSO_4 \cdot 4\,H_2O$) were identified instead of the heptahydrate phase. It was demonstrated that this is a subsequent process to the crystal being removed from solid-liquid equilibrium. With these considerations, it was possible to identify that phases melanterite and szomolnokite were properly formed when expected.

- Although it was not the objective of this work, prelminary morphology information of the crystals formed from the $FeSO_4 - H_2SO_4 - H_2O$ system was presented. Furthermore, we did not find in the literature a description of the morphology of crystals containing melanterite and/or szomolnokite from aqueous solutions. However, in comparison with articles that aim to describe the occurrence of these crystals naturally in different mines, the crystals found corresponded to the descriptions given.

- Compared to the thermodynamic model, the liquidus compositions obtained for the solutions associated with the $FeSO_4 - NiSO_4 - H_2O$ system showed differences of less than 1 wt% for iron and nickel sulfates using material balance. The divergence is 3 wt% when analyzing the composition of the solid in terms of each of the sulfates. Thus, it was possible to conclude that the experiments and model satisfactorily described the solid-liquid equilibrium.

- As with the sulfuric acid system, traces of rozenite were identified instead of melanterite in the structural analysis using XRD and Le Bail refinement for the $FeSO_4 - NiSO_4 - H_2O$ system. The heptahydrated nickel sulfate structure, morenosite, also dehydrated after being removed from the solid-liquid equilibrium, becoming nickelhexahydrite. Taking into account that this phenomenon is likely an artifact of the subsequent experimental handling procedures after solid-liquid equilibria was established, the experimentally identified crystal structures agreed with those predicted by the thermodynamic model, including in the miscibility gap region.

- In the $FeSO_4 - NiSO_4 - H_2O$ system, preliminary morphological information was presented and compared with that available in the literature. Similar to the system containing sulfuric acid, the melanterite present was compared with descriptions of its natural occurrence, but morenosite was compared with descriptions made from crystals obtained from aqueous solutions. In conclusion, the crystals formed in this work are compatible with the available descriptions.

- In summary, the findings from both systems demonstrated that the choice of characterization methodology and techniques led to satisfactory results in terms of solubility measurement. Evidently, the proposed objectives regarding the generation of new solu-

bility data for aqueous systems containing $FeSO_4 - H_2SO_4$ or $FeSO_4 - NiSO_4$ and analysis against literature or thermodynamic models were adequately achieved.

8.2 Limitations

The limitations exposed here are mainly associated with methodology, which, if resolved, could lead to an experimental protocol with more direct probing of solid-liquid equilibria. Here is a list of the main challenges faced during this work:

- The sensitivity of the systems to the presence of oxygen led to various trials and errors during the development of the methodology. The implementation of the glove bag, with an maximum of 2 vol% of O_2, to manipulate the solutions increased the time from 24 hours to a maximum of up to 2 weeks without signs of oxidation (yellowing). However, due to space limitations, not all equipment associated with its preparation and analysis could be placed inside the glove bag. It is believed that if the process from weighing the components to filtering the crystals could be carried out in an environment where oxygen levels are controlled, the time required for manipulating the solutions could be increased.

- Another challenge encountered as a consequence of the sensitivity of the systems studied was related to the dehydration of the crystals. The current configuration of the equipment used does not provide for humidity, temperature, and atmospheric control during analysis. Therefore, a change in the XRD configuration is necessary to make it compatible with the use of a sample holder that allows the environment in contact with the sample to be controlled.

- As for limitations associated with the interpretation of results, it is possible to highlight the calculations used for the AAS methodology described in 4.4.2. It is believed that conducting additional experiments to determine the density of individual solutions may lead to a more accurate calculation that can better describe the liquidus composition.

8.3 Future Research

As a suggestion for future research, the description of the miscibility gap region should be the subject of studies at variable temperatures. This would allow parametrization of higher accuracy thermodynamic models of the $FeSO_4 - NiSO_4 - H_2O$ system. Furthermore, studies can be conducted to explore the impacts of temperature on crystallization, as well

as parameters that affect crystal formation and the resulting morphology. This could help identify possible reasons why the signal associated with this crystallization was not observed through DSC. The use of innovative techniques for measuring chemical composition can be adopted, such as laser-induced breakdown spectroscopy. This technique allows in situ and real-time measurement, potentially facilitating the observation of the solid-liquid transition using any of the solubility measurement techniques discussed in this work. The study of the presence of solid solutions in phases other than heptahydrates is also be of interest, given that there is little literature exploring the $FeSO_4$–$NiSO_4$–H_2O system. In addition, the solid-liquid equilibria of other metal-sulfates solutions [4] should also be investigated in the effort to allow hydrometallurgical process optimization. It would be interesting to employ the results of solid-liquid equilibria studies to optimize the chemical precipitation steps during treatment of a real recycling residue.

REFERENCES

[1] F. Larouche, F. Tedjar, K. Amouzegar, G. Houlachi, P. Bouchard, G. P. Demopoulos, and K. Zaghib, "Progress and status of hydrometallurgical and direct recycling of li-ion batteries and beyond," *Materials*, vol. 13, no. 3, p. 801, Feb. 2020.

[2] J. J. Roy, S. Rarotra, V. Krikstolaityte, K. W. Zhuoran, Y. D. Cindy, X. Y. Tan, M. Carboni, D. Meyer, Q. Yan, and M. Srinivasan, "Green recycling methods to treat lithium-ion batteries e-waste: A circular approach to sustainability," *Advanced Materials*, vol. 34, no. 25, 10 2021. [Online]. Available: https://doi.org/10.1002/adma.202103346

[3] H. Bae and Y. Kim, "Technologies of lithium recycling from waste lithium ion batteries: a review," *Materials Advances*, vol. 2, no. 10, pp. 3234–3250, 1 2021. [Online]. Available: https://doi.org/10.1039/d1ma00216c

[4] Y. Ma, M. Svärd, X. Xiao, J. M. Gardner, R. T. Olsson, and K. Forsberg, "Precipitation and crystallization used in the production of metal salts for Li-Ion battery materials: a review," *Metals*, vol. 10, no. 12, p. 1609, 11 2020. [Online]. Available: https://doi.org/10.3390/met10121609

[5] Y. Zou, A. Chernyaev, S. Seisko, J. Sainio, and M. Lundström, "Removal of iron and aluminum from hydrometallurgical NMC-LFP recycling process through precipitation," *Minerals Engineering*, vol. 218, p. 109037, 10 2024. [Online]. Available: https://doi.org/10.1016/j.mineng.2024.109037

[6] Y. Ma, M. Svärd, J. Gardner, R. T. Olsson, and K. Forsberg, *Application of eutectic freeze crystallization in the recycling of Li-Ion batteries*, 1 2021. [Online]. Available: https://doi.org/10.1007/978-3-030-65489-4_1

[7] W. M. Haynes, D. R. Lide, and T. J. Bruno, Eds., *CRC Handbook of Chemistry and Physics*. CRC Press, 6 2016. [Online]. Available: https://doi.org/10.1201/9781315380476

[8] W. F. Linke and A. Seidell, *Solubilities: inorganic and metal-organic compounds: a compilation of solubility data from the periodical literature*. D. Van Nostrand Company, 1958.

[9] Y. Ma, M. Svärd, X. Xiao, S. A. Sahadevan, J. Gardner, R. T. Olsson, and K. Forsberg, "Eutectic freeze crystallization for recovery of $NiSO_4$ and $CoSO_4$ hydrates from sulfate solutions," *Separation and Purification Technology*, vol. 286, p. 120308, 12 2021. [Online]. Available: https://doi.org/10.1016/j.seppur.2021.120308

[10] E. J. Reardon, "Ion Interaction Model Applied to Equilibria in the $NISO_4-H_2SO_4-H_2O$ System," *American Chemical Society*, vol. 93, pp. 4630–4636, 12 1988.

[11] G. Agde and H. Barkholt, "Untersuchunhen uber die trennung von kupfervitriol und eisenvitriol durch kristallisation," *Angew. Chem.*, 1926.

[12] F. Fraenckel, "Uber die existenzgebiete der ferrousulfat-hydrate," *Anorg. Chem.*, 1907.

[13] M. Etard, "Recherches expérimentales sur les solutions saturées." *Ann. Chim. Phys.*, 1894.

[14] W. Bullough, T. A. Canning, and M. I. Strawbridge, "The solubility of ferrous sulphate in aqueous solutions of sulphuric acid," *Journal of Applied Chemistry*, vol. 2, no. 12, p. 703–707, Dec. 1952. [Online]. Available: https://doi.org/10.1002/jctb.5010021207

[15] F. K. Cameron, "The solubility of ferrous sulphate," *Journal of Physical Chemistry*, vol. 34, no. 4, p. 692–710, Apr. 1930. [Online]. Available: https://doi.org/10.1021/j150310a002

[16] J. Zhou, Y. Zeng, G. P. Demopoulos, C. Li, and Z. Li, "Phase transition of $FESO_4 \cdot 7\,H_2O$ to $FESO_4 \cdot H_2O$ in the H_2SO_4-H_2O–HCL system by modeling solubility," *ACS Sustainable Chemistry & Engineering*, vol. 6, no. 2, p. 2207–2219, Dec. 2017. [Online]. Available: https://doi.org/10.1021/acssuschemeng.7b03627

[17] Belopol'skii, Kolichev, and Shpunt, "$FeSO_4-H_2SO_4-H_2O$ system III.: The solubility of ferrous sulfate heptahydrate in aqueous solutions of sulfuric acid at temperatures from 10 to 50°c." *Zhur. Priklad. Khim.*, vol. 21, no. 8, p. 794–801, 1948.

[18] K. A. Kobe and R. E. Fredrickson, "Waste pickle liquor. ferrous sulfate-sulfuric acid-water," *Industrial & Engineering Chemistry Chemical & Engineering Data Series*, vol. 1, no. 1, p. 13–17, Jan. 1956. [Online]. Available: https://doi.org/10.1021/i460001a003

[19] M. V. Charykova, V. G. Krivovichev, and W. Depmeier, "Thermodynamics of arsenates, selenites, and sulfates in the oxidation zone of sulfide ores. II. Systems M_1, $M_2//SO_4^{2-}-H_2O$ (M_1, M_2= Fe^{2+}, Fe^{3+}, Cu^{2+}, Zn^{2+} , Pb^{2+}, Ni^{2+}, Co^{2+}, H^+) at 25°C,"

Geology of Ore Deposits, vol. 52, no. 8, pp. 701–710, 12 2010. [Online]. Available: https://doi.org/10.1134/s1075701510080027

[20] C. Balarew, V. Karaivanova, and S. Aslanian, "Isomorphiebeziehungen bei den heptahydratsulfaten von einigen zweiwertigen metallen (Mg^{2+}, Zn^{2+}, Ni^{2+}, Fe^{2+}, Co^{2+})," *Kristall und Technik*, vol. 8, no. 1-3, pp. 115–125, 1973.

[21] E. Königsberger, "Editorial: Guidelines for the measurement of Solid–Liquid Solubility Data at Atmospheric Pressure," *Journal of Chemical & Engineering Data*, vol. 64, no. 2, pp. 381–385, 2 2019. [Online]. Available: https://doi.org/10.1021/acs.jced.8b01263

[22] R. Cohen-Adad and M. Cohen-Adad, *Solubility of solids in liquids*. John Wiley & Sons, 3 2003. [Online]. Available: https://doi.org/10.1002/0470867833

[23] H. K. Zimmerman, "The experimental determination of solubilities," College of Arts and Sciences, University of Kentucky, Lexington, Kentucky, Tech. Rep., 7 1951.

[24] Z. Huang, S. Staufenbiel, and R. Bodmeier, "Combination of co-crystal and nanocrystal techniques to improve the solubility and dissolution rate of poorly soluble drugs," *Pharmaceutical Research*, vol. 39, no. 5, pp. 949–961, 5 2022. [Online]. Available: https://doi.org/10.1007/s11095-022-03243-9

[25] A. Chettri, A. Subba, G. P. Singh, and P. P. Bag, "Pharmaceutical co-crystals: A green way to enhance drug stability and solubility for improved therapeutic efficacy," *Journal of Pharmacy and Pharmacology*, vol. 76, no. 1, pp. 1–12, 11 2023. [Online]. Available: https://doi.org/10.1093/jpp/rgad097

[26] J. Sun, L. Wang, and G. Yu, "Effects of Na, Ca, Mg, and Al chloride salts on dissolution and phase stability of calcium sulfate dihydrate in aqueous solutions at 278.15 K to 308.15 K," *Journal of Chemical & Engineering Data*, vol. 60, no. 9, pp. 2559–2566, 7 2015. [Online]. Available: https://doi.org/10.1021/acs.jced.5b00005

[27] E. Reardon and R. Beckie, "Modelling chemical equilibria of acid mine-drainage: The $FeSO_4-H_2SO_4-H_2O$ system," *Geochimica et Cosmochimica Acta*, vol. 51, no. 9, pp. 2355–2368, 1987.

[28] Belopol'skii and Urusov, "$FeSO_4-H_2SO_4-H_2O$ system II.: The solubility of ferrous sulfate heptahydrate in aqueous solutions of sulfuric acid at temperatures from -20 to 25°C." *Zhur. Priklad. Khim.*, vol. 21, no. 8, p. 794–801, 1948.

[29] D. Ait Amer, "Développement d'un protocole expérimental pour l'étude cinétique et thermodynamique de la dissolution des sulfates de fer et de cobalt dans le cadre du recyclage des batteries lithium-ion." Master's thesis, Polytechnique Montréal, Montreal, QC, 2023.

[30] E. Baka, J. E. Comer, and K. Takács-Novák, "Study of equilibrium solubility measurement by saturation shake-flask method using hydrochlorothiazide as model compound," *Journal of Pharmaceutical and Biomedical Analysis*, vol. 46, no. 2, pp. 335–341, 11 2007. [Online]. Available: https://doi.org/10.1016/j.jpba.2007.10.030

[31] T. Kousksou, A. Jamil, Y. Zeraouli, and J.-p. Dumas, "Equilibrium liquidus temperatures of binary mixtures from differential scanning calorimetry," *Chemical Engineering Science*, vol. 62, no. 23, pp. 6516–6523, 7 2007. [Online]. Available: https://doi.org/10.1016/j.ces.2007.07.008

[32] P. Atkins, J. De Paula, and J. Keeler, *Atkins' physical chemistry*. Oxford University Press, 12 2022. [Online]. Available: https://doi.org/10.1093/hesc/9780198847816.001.0001

[33] M. D. Koretsky, *Engineering and Chemical thermodynamics*, 2nd ed. Wiley, 1 2013.

[34] K. S. Pitzer, *Activity Coefficients in Electrolyte Solutions*. CRC Press, 1991.

[35] A. M. Michałowska-Kaczmarczyk, A. Spórna-Kucab, and T. Michałowski, "Solubility Products and Solubility Concepts," *InTech eBooks*, 8 2017. [Online]. Available: https://doi.org/10.5772/67840

[36] M. Prieto, "Thermodynamics of solid solution-aqueous solution systems," *Reviews in Mineralogy and Geochemistry*, vol. 70, no. 1, pp. 47–85, 2009.

[37] K. S. Pitzer, "Thermodynamics of electrolytes. I: Theoretical basis and general equations," *The Journal of physical chemistry*, vol. 77, no. 2, pp. 268–277, 1973.

[38] P. Kobylin, T. Kaskiala, and J. Salminen, "Modeling of H_2SO_4−$FeSO_4$−H_2O and H_2SO_4−$Fe_2(SO_4)^3$−H_2O systems for metallurgical applications," *Industrial & Engineering Chemistry Research*, vol. 46, no. 8, pp. 2601–2608, 3 2007. [Online]. Available: https://doi.org/10.1021/ie061302y

[39] L. Kaufman and H. Bernstein, *Computer calculation of phase diagrams with special reference to refractory metals*. Academic Press, 1 1970.

[40] C. W. Bale, E. Bélisle, P. Chartrand, S. Decterov, G. Eriksson, K. Hack, I.-H. Jung, Y.-B. Kang, J. Melançon, A. Pelton *et al.*, "Factsage thermochemical software and databases—recent developments," *Calphad*, vol. 33, no. 2, pp. 295–311, 2009.

[41] P. Kobylin, H. Sippola, and P. Taskinen, "Thermodynamic modelling of aqueous Fe (II) sulfate solutions," *Calphad*, vol. 35, no. 4, pp. 499–511, 2011.

[42] J. L. Jambor, D. K. Nordstrom, and C. N. Alpers, "Metal-sulfate Salts from Sulfide Mineral Oxidation," *Reviews in Mineralogy and Geochemistry*, vol. 40, no. 1, pp. 303–350, 1 2000. [Online]. Available: https://doi.org/10.2138/rmg.2000.40.6

[43] P. Kobylin, "Thermodynamics of concentrated aqueous solution of $NiSO_4$," in *EMC, European Metallurgical Conference 2011*. GDMB Verlag, 2011, pp. 957–974.

[44] M. S. Rutstein, "Nickeloan melanterite from sudbury basin," *American Mineralogist*, vol. 65, no. 9-10, pp. 968–969, 1980.

[45] B. Morgan and O. Lahav, "The effect of pH on the kinetics of spontaneous Fe(II) oxidation by O_2 in aqueous solution – basic principles and a simple heuristic description," *Chemosphere*, vol. 68, no. 11, pp. 2080–2084, 3 2007. [Online]. Available: https://doi.org/10.1016/j.chemosphere.2007.02.015

[46] F. Yuan, "Study on kinetics of Fe (II) oxidized by air in $FeSO_4$–H_2SO_4 solutions," *Minerals Engineering*, vol. 121, pp. 164–168, 3 2018. [Online]. Available: https://doi.org/10.1016/j.mineng.2018.03.013

[47] R. E. Huffman and N. Davidson, "Kinetics of the ferrous Iron-Oxygen reaction in sulfuric acid solution," *Journal of the American Chemical Society*, vol. 78, no. 19, pp. 4836–4842, 10 1956. [Online]. Available: https://doi.org/10.1021/ja01600a004

[48] R. Raiseliene, G. Linkaite, A. Ezerskyte, and I. Grigoraviciute, "Tailored morphology and phase evolution of magnesium whitlockite granules via a Dissolution–Precipitation approach," *Applied Sciences*, vol. 15, no. 13, p. 7221, 6 2025. [Online]. Available: https://doi.org/10.3390/app15137221

[49] S. Hassanzadeh-Tabrizi, "Precise calculation of crystallite size of nanomaterials: A review," *Journal of Alloys and Compounds*, vol. 968, p. 171914, 8 2023. [Online]. Available: https://doi.org/10.1016/j.jallcom.2023.171914

[50] H. Toraya and R. Corporation, "Review of the direct derivation method: quantitative phase analysis with observed intensities and chemical composition data," Tech. Rep. 3, 4 2021.

[51] S. Baek, D. Setiawan, H. Lee, S. Lee, J. Pyun, S. Hong, and M. S. Chae, "Layered iron vanadate for High-Performance and stable cathode material for aqueous manganese batteries," *Advanced Science*, 4 2025. [Online]. Available: https://doi.org/10.1002/advs.202503006

[52] G. Cai, K. Y. Fung, K. M. Ng, and C. Wibowo, "Process development for the recycle of spent lithium ion batteries by chemical precipitation," *Industrial & Engineering Chemistry Research*, vol. 53, no. 47, pp. 18 245–18 259, 2014.

[53] V. A. Komornikov, N. I. Sorokina, N. A. Vasilyeva, D. S. Matveeva, and A. E. Voloshin, "Phase formation in the $NiSO_4-CoSO_4-H_2O$ system and specifications in the structures of single crystals of $Co_xNi_{(2-x)}(SO_4)_2 \cdot 12\,H_2O$," *Journal of Physics and Chemistry of Solids*, vol. 185, p. 111706, 2024.

[54] D. M. Marinova, E. N. Zhecheva, R. R. Kukeva, P. V. Markov, D. D. Nihtianova, and R. K. Stoyanova, "Mixed sodium nickel-manganese sulfates: Crystal structure relationships between hydrates and anhydrous salts," *Journal of Solid State Chemistry*, vol. 250, pp. 49–59, 2017.

[55] Y. Liu, Z. Wang, Y. Zhang, T. Wu, T. Zheng, B. Guo, G. Reiter, and J. Xu, "The size of critical secondary nuclei of polymer crystals does not depend on supersaturation," *Nature Communications*, vol. 16, no. 1, p. 3773, 2025.

[56] S. Black, L. Dang, C. Liu, and H. Wei, "On the measurement of solubility," *Organic process research & development*, vol. 17, no. 3, pp. 486–492, 2013.

[57] M. Lacalamita, G. Ventruti, G. Della Ventura, F. Radica, D. Mauro, and E. Schingaro, "In situ High-Temperature X-ray powder diffraction and infrared spectroscopic study of melanterite, $FeSO_4 \cdot 7\,H_2O$," *Minerals*, vol. 11, no. 4, p. 392, 4 2021. [Online]. Available: https://doi.org/10.3390/min11040392

[58] A. G. Mitchell, "The preparation and characterization of ferrous sulphate hydrates," *Journal of Pharmacy and Pharmacology*, vol. 36, no. 8, pp. 506–510, 8 1984. [Online]. Available: https://doi.org/10.1111/j.2042-7158.1984.tb04440.x

[59] A. M. Kul'kov and A. E. Glikin, "Replacement of Nickelhexahydrite with Retgersite: Polymorphic–Metasomatic Structures," *Geol. Ore Deposits*, vol. 49, pp. 821–826, 2007.

[60] M. Friesen, H. M. Burt, and A. Mitchell, "The dehydration of nickel sulfate," *Thermochimica Acta*, vol. 41, no. 2, pp. 167–174, 1980. [Online]. Available: https://www.sciencedirect.com/science/article/pii/004060318080061X

[61] I.-M. Chou and R. R. Seal, "Acquisition and evaluation of thermodynamic data for morenosite-retgersite equilibria at 0.1 MPa," *American Mineralogist*, vol. 88, no. 11-12, pp. 1943–1948, 2003. [Online]. Available: https://doi.org/10.2138/am-2003-11-1237

[62] J. Sánchez España and M. Diez Ercilla, *Geochemistry Research Advances*. Nova Science Publishers, Inc., 2008. [Online]. Available: https://www.researchgate.net/publication/232088519

[63] P. Gomes, T. M. F. Valente, J. A. Grande, and M. Cordeiro, "Occurrence of sulphate efflorescences in São Domingos mine," *Comunicações Geológicas*, 1 2017. [Online]. Available: https://repositorium.sdum.uminho.pt/bitstream/1822/65713/1/12_Gomes_WES2016.pdf

[64] I. B. Jenssen, O. Bøckman, J.-P. Andreassen, and S. Ucar, "The effect of reaction conditions and presence of magnesium on the crystallization of nickel sulfate," *Crystals*, vol. 11, no. 12, p. 1485, 11 2021. [Online]. Available: https://doi.org/10.3390/cryst11121485

[65] J. W. Anthony, R. A. Bideaux, K. W. Bladh, and M. C. Nichols, Eds., *Handbook of Mineralogy*. Chantilly, VA 20151–1110, USA: Mineralogical Society of America, 2005. [Online]. Available: http://www.handbookofmineralogy.org/

[66] A. Ulloa, F. Gázquez, A. Sanz-Arranz, J. Medina, F. Rull, J. M. Calaforra, G. Alvarado, M. Martínez, G. Avard, J. De Moor, and J. De Waele, "Extremely high diversity of sulfate minerals in caves of the Irazú Volcano (Costa Rica) related to crater lake and fumarolic activity," *International Journal of Speleology*, vol. 47, no. 2, pp. 229–246, 5 2018. [Online]. Available: https://doi.org/10.5038/1827-806x.47.2.2198

[67] R. Wiese, M. Powell, and W. Fyfe, "Spontaneous formation of hydrated iron sulfates on laboratory samples of pyrite- and marcasite-bearing coals," *Chemical Geology*, vol. 63, no. 1-2, pp. 29–38, 7 1987. [Online]. Available: https://doi.org/10.1016/0009-2541(87)90071-4